THE JOURNAL OF BIOLOGICAL CHEMISTRY VOL. 291, NO. 6, pp. 2731–2750, February 5, 2016

Identification of an Endogenously Generated Cryptic Collagen Epitope (XL313) That May Selectively Regulate Angiogenesis by an Integrin Yes-associated Protein (YAP) Mechano-transduction Pathway*

Received for publication, June 3, 2015, and in revised form, December 11, 2015 Published, JBC Papers in Press, December 14, 2015, DOI 10.1074/jbc.M115.669614

Jacquelyn J. Ames, Liangru Contois, Jennifer M. Caron, Eric Tweedie, Xuehui Yang, Robert Friesel, Calvin Vary, and Peter C. Brooks[1]

From the Maine Medical Center Research Institute, Center for Molecular Medicine, Scarborough, Maine 04074

Extracellular matrix (ECM) remodeling regulates angiogenesis. However, the precise mechanisms by which structural changes in ECM proteins contribute to angiogenesis are not fully understood. Integrins are molecules with the ability to detect compositional and structural changes within the ECM and integrate this information into a network of signaling circuits that coordinate context-dependent cell behavior. The role of integrin $\alpha v\beta 3$ in angiogenesis is complex, as evidence exists for both positive and negative functions. The precise downstream signaling events initiated by $\alpha v\beta 3$ may depend on the molecular characteristics of its ligands. Here, we identified an RGD-containing cryptic collagen epitope that is generated *in vivo*. Surprisingly, rather than inhibiting $\alpha v\beta 3$ signaling, this collagen epitope promoted $\alpha v\beta 3$ activation and stimulated angiogenesis and inflammation. An antibody directed to this RGDKGE epitope but not other RGD collagen epitopes inhibited angiogenesis and inflammation *in vivo*. The selective ability of this RGD epitope to promote angiogenesis and inflammation depends in part on its flanking KGE motif. Interestingly, a subset of macrophages may represent a physiologically relevant source of this collagen epitope. Here, we define an endothelial cell mechano-signaling pathway in which a cryptic collagen epitope activates $\alpha v\beta 3$ leading to an Src and p38 MAPK-dependent cascade that leads to nuclear accumulation of Yes-associated protein (YAP) and stimulation of endothelial cell growth. Collectively, our findings not only provide evidence for a novel mechano-signaling pathway, but also define a possible therapeutic strategy to control $\alpha v\beta 3$ signaling by targeting a pro-angiogenic and inflammatory ligand of $\alpha v\beta 3$ rather than the receptor itself.

Angiogenesis, the process by which new blood vessels form from pre-existing vessels, plays a critical role in normal and pathological events. Efforts are underway to more precisely define the interconnected mechanisms that control this crucial biological process to develop more effective strategies to control neovascular diseases (1, 2). Significant advances have been made in identifying molecular regulators of angiogenesis and their associated signaling pathways (3–5). A more precise understanding of angiogenic signaling pathways and the networks of regulatory feedback loops operating within distinct cellular compartments has provided important clues to help explain the modest clinical impact of many current anti-angiogenic strategies (1–5). For example, although vascular endothelial growth factor (VEGF) induces pro-angiogenic signaling leading to enhanced endothelial cell migration, growth, and survival, VEGF-induced blood vessels are often characterized as immature, unstable, and leaky and can regress in the absence of additional signaling events (6). VEGF stimulation under specific circumstances may lead to inhibition of angiogenesis in the context of altered PDGF signaling due to disruption of pericyte recruitment (6). These unexpected findings provide evidence of a negative role for the VEGF/VEGFR signaling during new vessel development (6). Similarly, studies have provided evidence for both a positive and a negative role for integrin $\alpha v\beta 3$ in angiogenesis (7–9). For example, multiple pro-angiogenic roles have been proposed for $\alpha v\beta 3$ as cyclic arginine-glycine-aspartic acid (RGD)-containing peptides and antibodies targeting this integrin inhibit angiogenesis in animal models (10–12). In contrast, enhanced angiogenesis was detected in tumors growing in $\alpha v\beta 3$ null mice (13). Interestingly, reduced pathological angiogenesis was detected in transgenic mice expressing signaling-deficient $\beta 3$-integrin, which resulted in part from defective recruitment of bone marrow-derived cells rather than specific endothelial cell defects (14). Moreover, new evidence suggests that $\beta 3$-integrin may play a more prominent role in the early stages of angiogenesis when new vessels begin to form, as reduction in endothelial cell expression of $\beta 3$-integrin impaired early stage pathological angiogenesis, but it had little effect on later maturation stages once vessels had formed (15). These studies, together with many others, suggest $\alpha v\beta 3$-mediated regulation of angiogenesis is complex, temporally regulated, and is not solely dependent on adhesive events but also involves downstream signaling, the consequences of which may depend on the cell type and composition of the local extracellular microenvironment (4, 9, 12, 16). Given the opposing biological

* This work was supported by National Institutes of Health Grants CA91645 (to P. C. B.), HL65301 (to R. F.), HL083151 and P20RR15555 (to C. V.), P20 RR181789 (Bioinformatics Core to D. M. Wojchowski), and 5P30GM103392 (to R. F.) and by the Holden Agency and Maine Medical Center. P. C. B. and C.V. hold an equity interest in CryptoMedix, LLC. The content is solely the responsibility of the authors and does not necessarily represent the official views of the National Institutes of Health.

[1] To whom correspondence should be addressed: Maine Medical Center Research Institute, Center for Molecular Medicine, 81 Research Dr. Scarborough, ME 04074. Tel.: 207-396-8239; Fax: 207-396-7669; E-mail: brookp1@mmc.org.

responses observed following modulation of some angiogenic regulatory molecules, it is not surprising that anti-angiogenic strategies based on targeting these factors have met with limited clinical success.

Given the importance of integrin-extracellular matrix (ECM)[2] interactions in modulating the intensity and specificity of growth factor signaling (1–5, 17, 18), it is important to define how diverse components within the local vascular microenvironment function cooperatively to regulate angiogenesis. Interestingly, distinct $\alpha v\beta 3$ ligands may stimulate opposing biological outcomes (7–15). For example, certain NC1 domains of collagen may bind $\alpha v\beta 3$ and induce pro-apoptotic responses, whereas binding of other $\alpha v\beta 3$ ligands may promote cell growth and survival (19–22). Given these findings and the complex biological effects observed following direct targeting of $\alpha v\beta 3$, an alternative therapeutic approach to control signaling from $\alpha v\beta 3$ might involve specific targeting of the pro-angiogenic ligands of $\alpha v\beta 3$ rather than directly targeting the receptor itself. Proteolytic remodeling of the ECM can generate integrin binding cryptic epitopes that play functional roles in angiogenesis, including the cryptic epitope present in multiple types of collagen that we have termed HU177, containing the amino acids, leucine, proline, and glycine (LPG*X*PG), where *X* can represent any amino acid and a second cryptic collagen epitope termed HUIV26, which is present in collagen type IV (21–23). Although the HUIV26 epitope is recognized by $\alpha v\beta 3$, it is not specifically composed of an RGD motif (21). Given the importance of RGD sequences in mediating some integrin-dependent interactions and the roles of amino acids flanking the core RGD motif in establishing integrin-binding specificity and affinity (24–27), we sought to determine whether RGD motifs within collagen differentially regulate angiogenesis. Sequence analysis of collagen type I revealed that five different cryptic RGD motifs are present, each with unique flanking sequences. Surprisingly, the C-terminal KGE flanking sequence of one of these RGD motifs is highly conserved in species as diverse as *Xenopus* and man. In contrast, significant sequence and positional variation exists within the other flanking sequences among different species.

Here, we provide evidence that an RGDKGE containing cryptic collagen epitope can be generated by a subset of macrophages, and this motif but not other RGD peptides may promote rather than inhibit angiogenesis. These novel findings are surprising given the wealth of experimental data indicating the high concentration of RGD peptides inhibit rather than induce angiogenesis (11, 28, 29). A growing body of evidence now suggests that low concentrations of certain RGD peptides may actually enhance angiogenesis and tumor growth (30), which may explain at least in part the minimal impact of cyclic RGD peptide antagonists of $\alpha v\beta 3$ and $\alpha v\beta 5$ in human clinical trials (31). Our current studies provide new evidence suggesting that in addition to variations in concentrations that may alter the biological response of certain RGD peptides, the specific composition of the amino acids C-terminal to the RGD motif within naturally occurring epitopes may confer unique pro-angiogenic and inflammatory activity. Taken together, our studies are consistent with a novel mechanism by which the RGDKGE collagen epitope may induce angiogenesis and inflammation by stimulating mechanical activation of $\alpha v\beta 3$ leading to Src-dependent phosphorylation of p38 MAPK that promotes nuclear accumulation of the Yes-associated protein (YAP) and enhances endothelial cell growth.

Experimental Procedures

Reagents, Kits, Chemicals, and Antibodies—Ethanol, methanol, acetone, bovine serum albumin (BSA), crystal violet, phosphate-buffered saline (PBS), purified human collagen type IV and collagen type I, AMPA, 3,3,5,5′-tetramethylbenzidine, phosphatase inhibitor mixture, and CA (cortisone acetate) were from Sigma. MMP2 was from Chemicon/Millipore (Billerica, MA). FBS was from Science Cell (Carlsbad, CA). Fibroblast growth factor-2 (FGF-2) was obtained from R&D Systems (Minneapolis, MN). Nuclear/cytoplasmic fractionation kit was from Thermo Scientific (Waltham, MA). p38 MAPK inhibitor SB202190 was obtained from Calbiochem. RIPA buffer, protease inhibitor, and Src inhibitor (PP2) were from Santa Cruz Biotechnology (Santa Cruz, CA). HRP-labeled anti-biotin was from Southern Biotechnology (Birmingham, AL). Anti-vWf antibody was from Pharmingen. Antibodies directed to p38 MAPK, phospho-p38 MAPK (Thr-180/Tyr-182), Src, and phospho-Src (Tyr-416) were from Cell Signaling Technology (Danvers, MA). Antibodies against tubulin, TATA-binding protein (TBP), YAP, $\beta 3$, and phospho-$\beta 3$ (Tyr-747) were from Santa Cruz Biotechnology. Anti-Igfbp4, anti-total, and phosphorylated JNK and anti-MMP9 antibodies were obtained from Abcam (Cambridge, MA). Function blocking antibodies P4C10 (anti-$\beta 1$), LM609 (anti-$\alpha v\beta 3$), and P1F6 (anti-$\alpha v\beta 5$) were from R&D Systems (Minneapolis, MN). HRP-conjugated secondary antibodies were from Promega (Madison, WI). Anti-collagen type I antibody was from Rockland (Limerick, PA), and anti-collagen type IV was from Millipore (Billerica, MA). Mouse monoclonal antibodies XL313 and XL166 were developed in our laboratory. Alexa-488, Alexa-594, streptavidin Alexa-594, and phalloidin Alexa-594-labeled antibodies were from Invitrogen. Unlabeled and biotin-labeled synthetic collagen RGD-containing peptides (P-1, CKGDRGDAPGC; P-2, CQGPRGDKGEC; P-3, CAGSRGDGGPC; P-4, CQGIRGDKGE; P-5, CRGPRGDQGPC) and peptide control (P-C, CQGPSGAPGEC) were obtained from QED Biosciences (San Diego, CA).

Generation of Hybridomas Producing Antibodies Reactive with RGD-containing Collagen Peptides—C57BL/6 mice were immunized (100 μg/mouse) every 3 weeks with synthetic RGD-containing collagen peptides (described in Table 1) that were conjugated to keyhole limpet hemocyanin carrier protein. Serum samples were analyzed for reactivity with immobilized RGD containing peptides by solid phase ELISA. Spleen cells from mice exhibiting strong immunoreactivity to the RGD containing collagen peptides were fused with myeloma cell line SP-20 by standard techniques. Hybridoma clones expressing antibodies exhibiting differential binding to RGD-containing

[2] The abbreviations used are: ECM, extracellular matrix; YAP, Yes-associated protein; TBP, TATA-binding protein; HUVEC, human umbilical vein endothelial cell; HRMVEC, human retinal microvascular endothelial cell; HMVEC, human microvascular endothelial cell; CAM, chick chorioallantoic membrane; CM, conditioned medium; CA, cortisone acetate; MMP, matrix metalloproteinase; P-C, peptide control; vWF, von Willebrand factor.

peptides were isolated following ELISA screening and subcloned by limiting dilution.

Cells and Cell Culture—RAW 264.7 and THP-1 cells were from ATCC (Manassas, VA) and cultured in DMEM and RPMI 1640 medium, respectively, in the presence of 10% FBS, 1.0% penicillin/streptomycin, and 1.0% sodium pyruvate. Immortalized BV-2 cells (32) were a gift from Dr. Ling Cao (University of New England, Biddeford, ME) and were cultured in DMEM with 10% FBS, 1.0% penicillin/streptomycin, and 1.0% sodium pyruvate. Human dermal fibroblasts were obtained from Science Cell (Carlsbad, CA) and cultured in fibroblast growth medium with 2.0% FBS and used between passages 4 and 9. Human retinal microvascular endothelial cells (HRMVECs) were obtained from Applied Cell Biology Institute (Kirkland, WA) and cultured in EBM2 supplemented with EGM-2 growth factors. Human umbilical vein endothelial cells (HUVECS) and human microvascular endothelial cells (HMVECS) were obtained from ATCC (Manassas, VA) and cultured in EBM2 with supplemental growth factors EGM-2 or EGM-2MV, respectively. All endothelial cell growth media contained 2% FBS, 1.0% penicillin/streptomycin, and 1.0% sodium pyruvate and were used experimentally between passages 3 and 9. For collection of conditioned media, cells were cultured in basal media under serum-free conditions for 24 h. Conditioned media were collected and concentrated 10× using an Amicon Ultracell, 3-kDa centrifugal ultrafiltration cartridge.

Cell Adhesion Assays—RGD peptides (P-1, P-2, P-3, P-4, P-5, and P-C) were immobilized (1–100 μg/ml) to wells. HUVEC, HMVEC, HRMVEC, and human dermal fibroblasts cells were suspended in adhesion buffer (RPMI 1640 medium containing 1 mM $MgCl_2$, 0.2 mM $MnCl_2$, and 0.5% BSA) and 1×10^5 cells were seeded into the wells in the presence or absence of P4C10, LM609, P1F6, or control antibodies (100 μg/ml). Cells were allowed to attach for 25 min at 37 °C. Media containing nonattached cells were aspirated, and attached cells were washed with PBS and stained with crystal violet (19). Cell adhesion was quantified by measuring the optical density of eluted dye (19). Adhesion assays were completed at least three times with triplicate wells.

Collagen Proteolysis and Solid Phase Binding Assays—Collagen type I and collagen type IV were heat-denatured for 15 min and then incubated with APMA-activated MMP2 for 0.5, 1, 4, 8, and 20 h, at 37 °C, followed by a 5-min boil to deactivate remaining MMP. For solid phase ELISAs, synthetic RGD-containing collagen peptides (P-1, P-2, P-3, P-4, P-5, and P-C) were immobilized (1.0 ng/ml to 100 μg/ml) to wells or wells were coated with 10 μg/ml native or MMP2-proteolyzed collagen type I or type IV. Wells were blocked with 1% BSA in PBS for 1 h and then incubated with 1 μg/ml mAbs XL313 or XL166 for 1 h, washed, and incubated with anti-mouse HRP-conjugated antibodies (1:5000). Bound mAbs were detected with a 3,3,5,5′-tetramethylbenzidine substrate as per the manufacturer's instructions and quantified via spectrometer measurements. All assays were carried out at least four times in triplicate wells.

Chick Chorioallantoic Membrane (CAM) Inflammation and Angiogenesis Assays—The CAM assays were carried out essentially as described with some modifications (19). Briefly, for all experiments CAMs of 10-day-old chick embryos obtained from Charles River (North Franklin, CT) were separated from the shell membrane. Filter discs were either non-treated (inflammation assays), pretreated (angiogenesis assays) with CA (3.0 mg/ml) containing RPMI 1640 medium only, or FGF-2 (40 ng). CAMs were either non-treated or treated topically with mAb XL313, XL166, or a nonspecific control antibody (10 μg/embryo every 24 h for three consecutive treatments). For peptide induction experiments, CAMs were stimulated with 100 ng/ml of the RGD peptides (P-1, P-2, P-4, or P-C) in the presence or absence of the p38 MAPK inhibitor, SB202190 (10 μM). At the end of the incubation period, the embryos were sacrificed, and the CAM tissues were analyzed. Angiogenesis was quantified by counting the number of angiogenic branching blood vessels within the area of the filter disc. The angiogenic index was determined by subtracting the mean number of blood vessel branch points from untreated CAMs from each experimental condition as we described previously (19). Eight to twelve embryos were used per condition, and experiments were repeated at least three times.

Transfections of CAM Tissues and Quantitative PCR Analysis—Chick CAM angiogenesis assays were performed as described previously with slight modification. Briefly, FGF-2-containing filter discs were first placed onto dropped CAM. The siRNA duplex-Lipofectamine RNAiMax complexes were formed by mixing 20 pmol of siRNA (TriFECTa™ dicer-substrate kit (IDT)) and 3 μl of Lipofectamine RNAiMAX (Life Technologies), each in 50 μl of Opti-MEM medium. The three Dicer-Substrate 27-mer siRNAs to chicken Yap designed and purchased from IDT with sequences of 5′-AGCACAGAUAGCGGACUUAGCAUGA-3′, 5′-UGACUACAAAUAGUUCUGAUCCCTT-3′, and 5′-GCCACCAAGCCAGAUAAAGAGAGTT-3′ were applied to the filter discs in a total volume of 40 μl. After 72 h, individual CAM tissues were dissected, photographed, and frozen for further analyses. For quantitative PCR analysis, the cDNA templates of individual tissues were generated using iScript™ reverse transcription supermix (Bio-Rad). Quantitative PCR was performed using SsoAdvanced™ Universal SYBR Green Supermix (Bio-Rad) according to the manufacturer's protocol. Chicken Yap expression was analyzed by The CFX96™ optical reaction module with primers specific for chicken Yap (forward primer, AGCCAAAGTGCTCCAGTGAA-3′, and reverse primer, CTACGGAGAGCCAATTCCTGC-3′) and 18S (forward primer, GTTCAGCCACCCGAGATTGA-3′, and reverse primer, CCCATCACGAATGGGGTTCA-3′). Experiments were performed twice.

Isolation of Primary CAM Macrophages and Staining Analysis—CAM tissues were dissected, and minced tissue fragments were incubated at 37 °C for 60 min in 10 ml of dissociated medium containing collagenase/Dispase (Roche Applied Science, at 1 mg/ml) and 20% fetal bovine serum in RPMI 1640 medium. The digested tissues were poured through a 100-μm cell strainer into a 50-ml sterile tube and incubated on ice for 4 min to allow settling of debris. The supernatants were transferred into a new tube and spun at 300 × *g* for 10 min. Red cells were lysed and removed by ACK lysing buffer (Lonza). The cell pellets were washed twice in 10% RPMI 1640 medium. The final suspension of cells was seeded onto glass slides and incubated at 37 °C for 60 min to allow macrophages to adhere. Non-adher-

ent cells were removed by PBS wash. Adhered cells were fixed in ice-cold methanol/acetone for 5 min.

Fixed adherent cells were washed with PBS and blocked with 1% normal goat serum and 2% BSA in TBS at room temperature for 1 h. The cells were then incubated in 2% BSA/TBS containing KUL anti-chick macrophage/monocytes antibody overnight at 4 °C. The slides were washed with TBS and incubated in 2% BSA/TBS containing Alexa Fluor 488 goat anti-mouse IgG at room temperature for 1 h. After washing, slides were incubated in avidin/biotin blocking solution according to the manufacturer's recommendation (Vector Laboratories) followed by 1-h incubation of biotinylated XL313 (20 μg/ml). Slides were washed and incubated with Alexa Fluor 594-conjugated streptavidin (Life Technologies, Inc.) for 1 h. Next, slides were rinsed with TBS, counter-stained with DAPI, and mounted with Fluoromount aqueous medium (Sigma).

Immunohistochemistry and Immunofluorescence Analysis—CAMs examined for accumulation of granulation tissue were harvested, fixed in 4% paraformaldehyde, paraffin-embedded and sectioned (4 μm), and stained with Giemsa. CAM tissues analyzed via immunofluorescence were harvested, embedded with OCT, snap-frozen, and sectioned (4 μM). Frozen sections were fixed in 50% methanol, 50% acetone, air-dried, and blocked with 2.5% BSA for 1 h at 37 °C. For expression of the XL313 and XL166 epitopes as well as monocyte/macrophages, FGF-2-stimulated CAM tissues were stained with mAbs XL313 XL166, (50 μg/ml), or KUL1 (1:250) and then incubated with Alexa-488-labeled secondary antibodies (1:2000 dilution). Co-staining of monocytes/macrophages and the mAb XL313-reactive epitope in FGF-2 stimulated CAMs was performed by sequential staining by first probing with KUL1 (1:250) and then with a biotin-conjugated mAb XL313 (50 μg/ml) and with secondary antibodies Alexa-488 and streptavidin Alexa-594 (1:2000), respectively. Using a similar strategy, sections of RGD peptide-treated CAM tissues were analyzed for phosphorylated p38 MAPK in angiogenic vessels by co-incubation of anti-phospho-p38 MAPK (1:50) and anti-vWf (1:500) antibodies. Subcellular localization of YAP was observed in HUVECS attached to P-2- and P-1-coated glass coverslips. Cells were allowed to attach for 15, 30, or 60 min in the absence of serum and were fixed with 4% paraformaldehyde. Fixed cells were washed and blocked with 2.5% BSA and stained with anti-YAP (1:200) and phalloidin (1:500). All sections and slides were counter-stained with DAPI. For staining and quantification of actin stress fibers, HUVECs were resuspended in adhesion buffer (RPMI containing 1 mM $MgCl_2$, 0.2 mM $MnCl_2$, and 0.05% serum) and allowed to bind for 30 min to peptide-coated coverslips. Cells were stained with phalloidin (1:500) and counter-stained with DAPI. The number of cells with actin stress fibers was counted per ×400 field, from 25 fields per condition. Experiments were complete three times.

Cell Proliferation Assays—HUVECs (WT, shYAP1, or control-transfected) or HRMVECs were plated at 2000 cells per well with complete EGM-2 media containing 2.0% FBS in the absence or presence of P-1, P-2, or P-C (100 μg/ml) and allowed to grow for 24 h. Cell growth was monitored using a BrdU or WST-1 assay kits according to the manufacturer's instructions. All assays were completed at least three times in triplicate wells.

Inhibitor Experiments—Endothelial cells (HUVECs or HRMVECs) were incubated in serum-free media with 1 mM $MgCl_2$, 0.2 mM $MnCl_2$ in the presence of an Src inhibitor, PP2 (10 μM), a p38 MAPK inhibitor SB202190 (10 μM), or vehicle only (DMSO) for 10 min at 37 °C. Treated cells were then seeded onto immobilized P-1 and P-2, and lysates were collected at 15 min.

Western Blot—Whole cell and CAM tissue lysates were collected in RIPA buffer supplemented with 1× protease inhibitor and 1× phosphatase inhibitor and were run on polyacrylamide gels using denaturing conditions. Prior to loading the gels, 6× sample buffer was added to each of the lysates (final concentration 1×) and boiled for 5 min. Twenty to 50 μg of total protein were loaded into each lane. For detection of proteins larger than 50 kDa, 10% gels were used; for proteins smaller than 50 kDa, 15% gels were used. Gels were run at 60 V until the dye front passed through the stacking gel, and then the voltage was increased to 100 V for the remainder of the separation. Precision Plus protein standards (Bio-Rad) were used to visualize migration. Protein was transferred to nitrocellulose membranes using a wet tank system and blocked for 1 h using 10% nonfat dried milk in Tris-buffered saline with 0.01% Tween 20 (TBS-T). Membranes were incubated with primary antibodies (anti-coll-I (1:250), anti-coll-IV (1:250), mAb XL313 (2 μg/ml), mAb XL166 (2 μg/ml), anti-β-actin (1:5000), anti-phospho-β3 (1:7000), anti-β3 (1:1000), anti-phospho-Src (1:500), anti-Src (1:500), anti-phospho-p38 MAPK (1:500), anti-p38 MAPK (1:2000), anti-YAP (1:500), anti-tubulin (1:2000), anti-TBP (1:1000)) in 5% BSA in TBS-T overnight at 4 °C with gentle agitation. Membranes were washed three times in TBS-T for 5 min. Blots were then incubated with HRP-conjugated secondary antibodies (1:15,000) in 1% nonfat milk in TBS-T for 1 h. Membranes were washed a second time as indicated above and exposed to chemiluminescent substrate for 3 min prior to exposure to autoradiography film in a dark room. Western blot bands were quantified using ImageJ software based on pixel intensity.

Transfections and Lentiviral Transductions—Raw cells were transfected with 1 μg of HuSH shRNA plasmids for collagen type and α2 using Amaxa cell line nucleofector kit V (program T024). Constructs expressing 21-nucleotide short hairpin RNAs (shRNA) targeting human YAP (shYAP) or non-targeting control (shNT, Sigma, SHC002) were used. Human-targeting shYAP1 lentiviral shRNA was obtained from the Thermo Scientific RNAi consortium (TRCN0000107625). Constructs were packaged into lentivirus, pseudotyped with the vesicular stomatitis virus glycoprotein. Transduction was performed by incubating cells with lentivirus, and stably transduced cells were subsequently used for studies. All cell lines were verified by morphology and mouse and human YAP-specific PCR. The efficacy of YAP knock down was determined to be between 70 and 80%. Endothelial cells were certified mycoplasma-negative by PCR (Lonza), and primary cell cultures were used within the indicated passage numbers. Cells were transduced and selected using puromycin.

Statistical Analysis—Statistical analysis was performed using the InStat statistical program for Macintosh computers. Data

TABLE 1

RGD-containing epitopes of collagen type I

Five different cryptic RGD-containing sites exist within human collagen type I, each with distinct flanking sequences. Synthetic peptides of these five sequences were generated and designated P-1 through P-5. Additionally, P-C was generated lacking the RGD tri-peptide motif. NA means not applicable.

Peptide	Amino acid sequence	Location
P-1	KGDRGDAPG	Col1a1 (742–750)
P-2	QGPRGDKGE	Col1a1 (1090–1098)
P-3	AGSRGDGGP	Col1a2 (774–782)
P-4	QGIRGDKGE	Col1a2 (1002–1010)
P-5	RGPRGDQGP	Col1a2 (819–827)
PC	QGPSGAPGE	NA

were analyzed for statistical significance using Student's *t* test. *p* values < 0.05 were considered significant.

Results

Cryptic RGD Containing Peptides from Collagen Type I Support Cell Adhesion—Studies have documented the capacity of ECM proteins containing the short amino acid sequence RGD to support interactions mediated by integrin receptors (33). The ability of cells to interact with RGD sites within the context of larger glycoproteins depends on many factors, some of which include the adjacent flanking sequences surrounding the core RGD tri-peptide as well as the geometrical configuration of the intact molecule and how these molecules are oriented within the context of the interconnected network of other ECM proteins (24, 25, 33). Flanking sequences immediately C-terminal to the RGD site can govern integrin selective binding (24, 25, 33). RGD motifs can be cryptic and inaccessible to cell surface receptors as is illustrated in the case of triple helical collagen (34). In this regard, five different cryptic RGD-containing sites exist within human collagen type I, each with distinct flanking sequences (Table 1).

Given the importance of the RGD tri-peptide motif, we sought to establish that the five distinct RGD sites represented by the five different collagen peptides shown in Table 1 could mediate cellular binding. To assess whether these cryptic collagen RGD motifs are redundant or whether the flanking sequences may help convey distinct properties, we synthesized each of the collagen type I RGD epitopes along with their associated flanking sequences. The five different RGD peptides were immobilized, and their ability to facilitate cell adhesion was examined. As shown in Fig. 1*A*, all five collagen RGD peptides (P1–P5) supported human umbilical vein endothelial cell (HUVEC) adhesion. In contrast to the RGD-containing peptides (P1–P5), peptide P-C in which the RGD motif of P-2 was replaced with SGA failed to support adhesion. To confirm the adhesion-promoting ability was not specific to only HUVECs, similar assays were carried out with HMVEC, HRMVEC, and human dermal fibroblasts. As expected, all endothelial cell lines and fibroblasts bound at various levels to the five RGD-containing collagen peptides, although the control peptide failed to support interactions (Fig. 1, *B–D*). In some cell types, especially HRMEVCs, P-5 supported enhanced levels of adhesion as compared with other RGD-containing peptides. To confirm that peptide P-5 promoted higher levels of adhesion to HRMVECs, we carried out similar adhesion assays over a dose range of immobilized peptide. Peptide P-5 supported enhanced levels of cell adhesion at all doses (1–100 μg/ml) tested (data not shown). To confirm similar absorption of the peptide to the wells, biotin-labeled versions of each of the peptides were immobilized, and the relative levels of absorbed peptide were quantified by ELISA. Minimal variations in peptide absorption were detected, and these small differences were not statistically significant (data not shown). These data suggest that although some differences were observed, all five RGD peptides were capable of supporting cell adhesion.

To study the cryptic collagen RGD epitopes in more detail, we generated monoclonal antibodies by immunizing mice with the RGD-containing collagen peptides described in Table 1. Hybridoma cell lines producing antibodies reactive with the RGD-containing peptides were examined by solid phase ELISA and subcloned. We isolated two distinct hybridoma clones producing antibodies with the ability to specifically discriminate between different RGD-containing epitopes. As shown in Fig. 1*E*, mAb XL313 specifically bound to collagen peptides P-2 and P-4 containing the conserved RGDKGE motif (Table 1), but they showed no significant reactivity with other RGD peptides, including P-1, P-3, or P-5. A second antibody termed XL166 recognized RGD-containing collagen peptides P-1, P-3, and P-5 but failed to bind significantly to the RGDKGE-containing peptides P-2 and P-4 (Fig. 1*F*). Neither mAb XL313 nor XL166 showed significant interaction with P-C.

mAb XL313 Exhibits Selective Binding for Proteolyzed Collagen Type I—We sought to determine whether mAb XL313 had the capacity to bind its RGD motif within the context of the full-length collagen molecule. To facilitate these studies, we first incubated denatured collagen type I or IV with MMP-2 for 12 h to generate proteolyzed collagen. As expected, MMP-2-mediated proteolysis of collagen type I and IV resulted in the generation of multiple fragments as indicated by Western blot analysis using antibodies specifically directed to either collagen type I (Fig. 2*A, left panel*) or collagen type IV (Fig. 2*A, right panel*). mAb XL313 specifically directed to the RGDKGE collagen sequence exhibited weak reactivity with intact collagen type I, and no reactivity with type IV collagen under denaturing and reducing conditions (Fig. 2*B*). Moreover, mAb XL313 demonstrated little reactivity to intact collagen type I or collagen type IV under non-denatured and non-reducing conditions of the ELISA while readily binding to proteolyzed collagen type I under these identical conditions (Fig. 2*C*). mAb XL313 failed to recognize other RGD-containing ECM proteins, including vitronectin or fibronectin (data not shown). To further examine the generation of the low molecular weight RGDKGE-containing collagen fragments, we examined a time course of MMP-2-mediated collagen proteolysis. Although mAb XL313 can recognize non-proteolyzed collagen type I that is structurally altered under denaturing and reducing conditions, MMP-2-mediated degradation of collagen type I resulted in a time-dependent generation of mAb XL313 reactive collagen fragments (Fig. 2*D*). The majority of the collagen was proteolyzed into mAb XL313-reactive fragments of ~14 to 16 kDa by 8 h. These findings are consistent with the notion that XL313 collagen epitopes appear to be cryptic within a structurally intact non-denatured collagen type I molecule and that proteolytic degra-

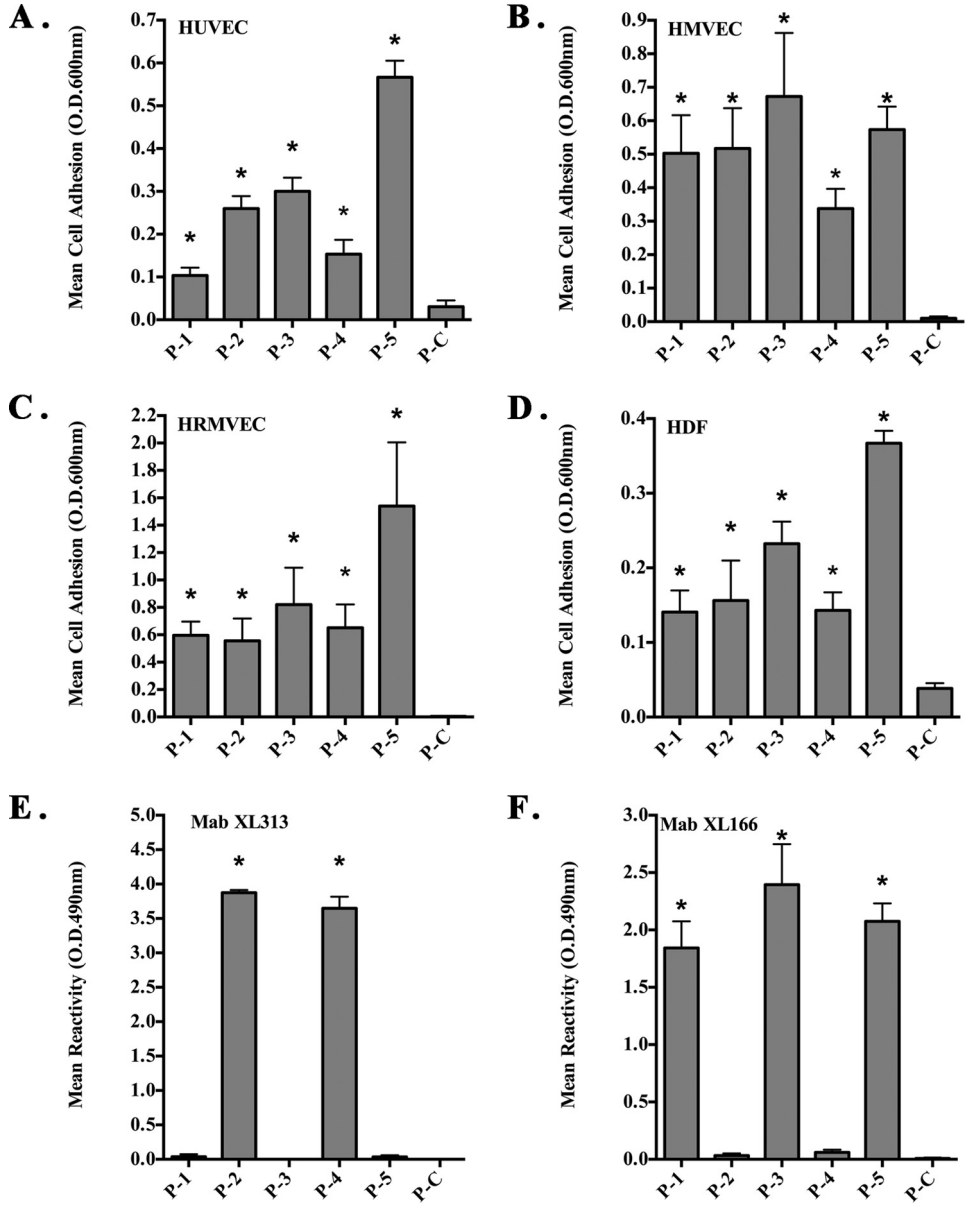

FIGURE 1. **Cryptic RGD-containing peptides from collagen type I support cell adhesion.** Peptides corresponding to the five different RGD-containing motifs of human collagen type I were synthesized with flanking cysteines and immobilized on non-tissue culture plates. The ability of stromal cells to attach to the peptides (*A–D*) or the ability of monoclonal antibodies to bind the immobilized peptides (*E* and *F*) was assessed. *A,* HUVEC adhesion to immobilized peptides. *B,* HMVEC adhesion to immobilized peptides. *C,* HRMVEC adhesion to immobilized peptides. *D,* human dermal fibroblast (*HDF*) adhesion to immobilized peptides. *E,* reactivity of mAb XL313 to immobilized peptides. *F,* reactivity of mAb XL166 to immobilized peptides. *Data bars* represent mean binding ± S.D. from at least three experiments each using triplicate wells. *, $p < 0.05$.

dation is required to more efficiently expose this hidden RGD-KGE-containing motif in non-denatured collagen.

Differential Roles of Cryptic RGD Collagen Motifs on Angiogenesis and Inflammation in Vivo—Our previous studies have shown that collagen remodeling within the vascular basement membrane can result in exposure of multiple non-RGD cryptic collagen sites, including the HUIV26 and HU177 epitopes that can play active roles in angiogenesis (21, 23). Given these findings and our current observations, we sought to determine whether distinct RGD-containing epitopes are exposed *in vivo*. First, to examine whether these RGD epitopes can be generated during angiogenesis, we used the chick chorioallantoic membrane (CAM) model (19). The CAMs of chick embryos were stimulated with FGF-2, and the generation of RGD-containing collagen epitopes was examined using mAbs XL313 and XL166. As shown in Fig. 3*A*, little mAb XL313 or XL166-reactive epitope could be detected in non-stimulated CAMs. In contrast, RGD-containing collagen epitopes (Fig. 3*A*, *green*) were readily detected in FGF-2-stimulated CAM tissues confirming the differential generation of RGD-containing epitopes recognized by these antibodies. Interestingly, mAb XL313- and XL166-reactive RGD epitopes did not exhibit a typical extracellular fibril collagen pattern, but rather they exhibited punctate distribution with both intracellular and scattered extracellular localization. The intracellular distribution is similar to the staining pattern of collagen degradation products previously documented within intracellular vesicles of macrophages (35).

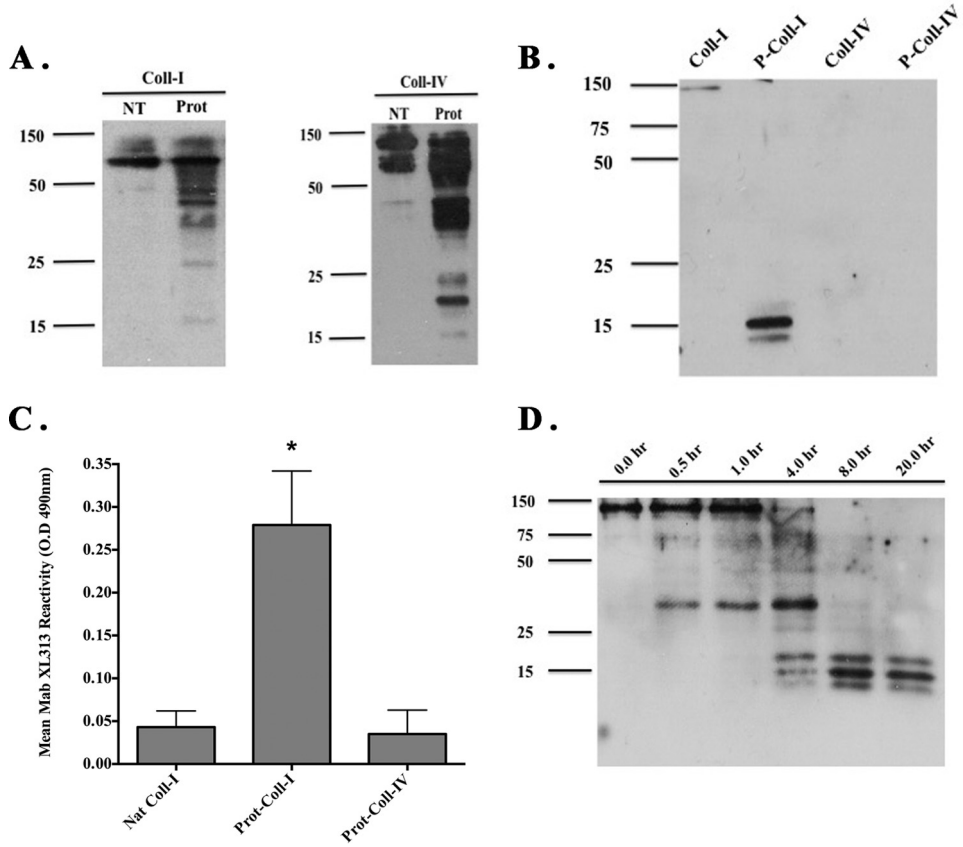

FIGURE 2. **mAb XL313 exhibits selective binding to proteolyzed collagen type I.** Purified collagen type I and collagen type IV were incubated with control buffer or activated MMP-2 over a time course and analyzed by Western blot (*A, B,* and *D*) or ELISA (*C*). *A,* Western blot analysis of control non-treated (*NT*) and MMP-2-proteolyzed (*Prot*) collagen type I (*left panel*) and collagen type IV (*right panel*) probed with anti-collagen type I-specific antibody (*left panel*) or anti-collagen type IV-specific antibody (*right panel*). *B,* Western blot analysis of control non-proteolyzed and MMP-2-proteolyzed collagen type I and type IV following 16 h of incubation and probed with mAb XL313 directed to the RGDKGE-containing collagen motif. *C,* detection of mAb XL313-reactive RGDKGE motif in non-proteolyzed (*Nat*) or MMP-2 proteolyzed (*Prot*) collagen by ELISA. *Data bars* indicate mean reactivity from triple wells ± S.D. *, $p < 0.05$. Experiments were completed at least three times with similar results. *D,* Western blot analysis of the time-dependent generation of the mAb XL313 reactive epitope of collagen type.

Given the generation of these distinct sets of RGD-containing epitopes, we next examined whether they may play active roles in regulating angiogenesis and inflammation. Angiogenesis was induced within the CAMs of 10-day-old chick embryos with FGF-2 using filter discs coated with CA to reduce growth factor-associated inflammation. As shown in Fig. 3*B*, treatment with mAb XL313 directed to the cryptic RGDKGE-containing epitope significantly ($p < 0.05$) inhibited FGF-2-induced angiogenesis by greater than 75% as compared with non-treated or control antibody. Surprisingly, mAb XL166 that specifically binds the remaining three distinct cryptic RGD collagen peptides (P-1, P-3, and P-5) had no effect. These surprising findings are consistent with the possibility that although distinct RGD-containing collagen epitopes are readily generated *in vivo*, they may not be functionally redundant.

The chick CAM has been routinely used to assess inflammation and granulation tissue formation, which are largely dependent on infiltration of chick heterophils (the avian equivalent of neutrophils), macrophages, and activated fibroblasts (36, 37). To study the potential differential biological impact of RGD epitopes, we examined FGF-2-induced inflammation by carrying out similar experiments in the absence of CA and quantifying CAM thickening. As shown in Fig. 3*C*, treatment with FGF-2 induced CAM inflammation as indicated by robust tissue thickening (*top panels*), extensive infiltration of inflammatory infiltrates as indicated by Giemsa stain (*middle panel*), and increased accumulation of monocytes and macrophages (*bottom panel*) following staining with an antibody directed to avian-specific monocytes and macrophages. Macrophage infiltration of the CAMs stimulated with FGF-2 was significantly ($p < 0.05$) enhanced by over 2-fold as compared with control (Fig. 3*D*) indicating that FGF-2-induced inflammation in this model is associated with the recruitment and accumulation of granulation tissue-associated macrophages as well as other stromal cells, including fibroblasts.

To examine whether the RGD-containing collagen epitopes play a role in the FGF-2-stimulated inflammatory response, we examined this FGF-2-induced inflammatory response in the presence or absence of anti-RGD-specific antibodies XL313 and XL166. Quantification indicated that FGF-2 stimulation in the absence of CA resulted in ~50% of the CAMs showing robust formation of thick granulation tissue (Fig. 3*E*). Treatment of CAMs with CA, a well documented anti-inflammatory agent, significantly ($p < 0.05$) reduced the percentage of CAMs exhibiting thickening by greater than 80% as compared with either no treatment or control antibody. Moreover, reduced

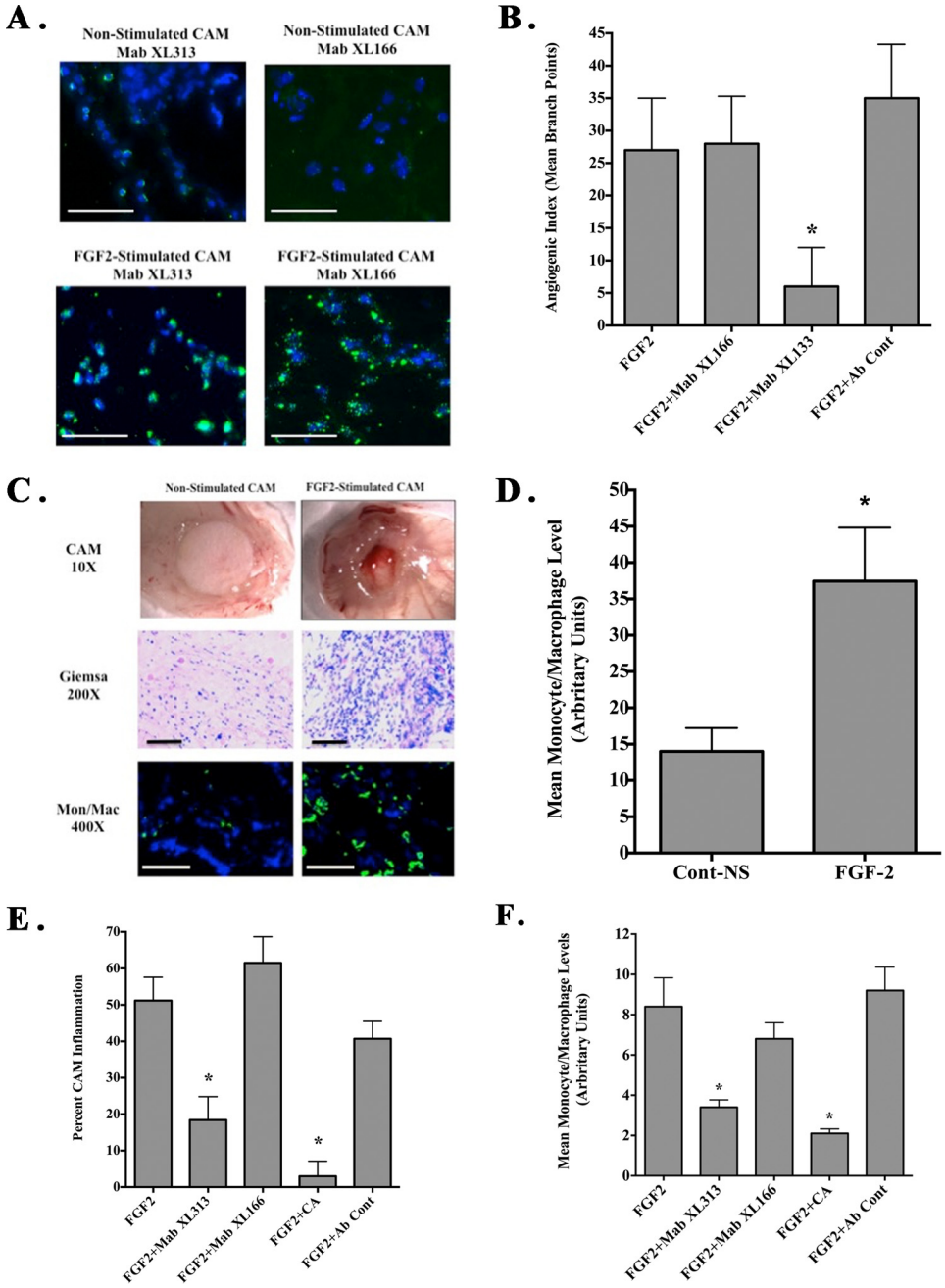

FIGURE 3. **Differential effects of cryptic RGD collagen motifs on angiogenesis and inflammation *in vivo*.** CAMs were either unstimulated or stimulated with FGF-2 in the presence or absence of CA. *A,* representative examples of unstimulated or FGF-2-stimulated CAM tissues stained with mAbs XL313 and XL166 (*green*). *Scale bars,* 50 μm. *B,* quantification of FGF-2-induced angiogenesis in the absence or presence of mAbs XL313, XL166, or nonspecific control antibody. *Data bars* represent mean number of angiogenic branching vessels ± S.E. from 8 to 10 animals per condition. Experiments were completed at least three times with similar results. *C,* unstimulated or FGF-2-stimulated CAMs in the absence of cortisone acetate. Representative examples of inflammatory CAM thickening (*top panel*), Giemsa-positive inflammatory infiltrates (*middle panel*), and infiltration of macrophages (*green*) following staining with anti-avian-specific macrophage marker KUL1 (*bottom panel*) are shown. *Scale bars,* 50 μm. *D,* quantification of relative macrophage infiltration following FGF-2 stimulation in the absence of CA. *Data bars* represent mean ± S.E. levels of KUL-expressing avian macrophages per ×100 microscopic field from five fields per CAM and 10 CAM per condition. *, $p < 0.05$. *E,* quantification of FGF-2 induced inflammation in the absence or presence of mAbs XL313, XL166, CA, or nonspecific control antibody. *Data bars* represent mean percentage inflammatory CAMs ± S.E. Experiments were completed at least three times with similar results. *, $p < 0.05$. *F,* quantification of relative macrophage infiltration. *Data bars* represent mean ± S.E. of the levels of KUL-expressing avian macrophages per ×400 microscopic field from 9 to 10 fields per CAM and five CAM per condition. *, $p < 0.05$.

levels of inflammatory infiltrates, including macrophages, were also observed (Fig. 3*F*). Interestingly, treatment of CAMs with mAb XL313 also significantly ($p < 0.05$) inhibited the number of CAMs exhibiting inflammation by ~75% as well as reducing the relative levels of inflammatory infiltrates as compared with controls (Fig. 3, *E* and *F*). In contrast, treatment of CAMs with mAb XL166 showed no significant ($p > 0.05$) impact. These data are consistent with our previous findings when examining angiogenesis suggesting a differential role for specific cryptic RGD epitopes *in vivo*.

Generation of XL313 Cryptic RGDKGE Epitope—During angiogenesis and inflammation, multiple cell types, including

endothelial cells, fibroblasts, and macrophages proteolytically remodel extracellular collagen creating a permissive microenvironment that facilitates stromal cell infiltration and new blood vessel growth. A variety of cells, including fibroblasts and endothelial cells, can express collagen, and moreover, partially degraded collagen can be internalized and further processed by activated M2-like macrophages leading to the generation of low molecular weight fragments (35, 38). Given the unique pattern of mAb XL313 immunoreactivity observed *in vivo*, we examined whether stromal cells associated with angiogenesis and inflammation could generate the RGDKGE-containing epitope. Whole cell lysates were prepared from fibroblasts and endothelial cells, and Western blotting was carried out. Although some mAb XL313-reactive species could be detected in lysates of endothelial cells and fibroblasts, the major immunoreactive species migrated between ~75 kDa and 28 kDa (Fig. 4*A, left panel*) indicating that these species were unlikely to represent intact collagen. In addition, minimal if any low molecular weight species was detected that might correspond to the major 14- to 16-kDa collagen fragments detected following MMP-2-mediated proteolysis. Interestingly, although a small amount of an ~20-kDa XL313-reactive species was detected in serum-free CM collected from HUVECS, we failed to detect significant levels of immunoreactive fragments in fibroblast CM (Fig. 4*A, right panel*). Given the minimal reactivity observed in these cell types known to express collagen and the fact that FGF-2 induced a strong angiogenic and inflammatory response in CAMs that was associated with an extensive infiltration of macrophages, we examined FGF-2-treated CAM tissues for the co-distribution of the XL313 epitope and macrophages. As shown in Fig. 4*B*, the XL313-reactive epitope (*red*) co-localized with a subset of macrophages (*green*) in FGF-2-stimulated CAMs. In similar studies, the XL313 reactive epitope localized with primary macrophages isolated from CAM tissues (data not shown), suggesting the possibility that a subset of macrophages may be at least one source of the XL313 collagen epitope. To study this possibility, we examined both whole cell lysates (Fig. 4*C, left panel*) and serum free CM (Fig. 4*C, right panel*) from three different macrophage-like cell lines. In contrast to endothelial cells and fibroblasts, strong immunoreactive species were readily detected in cell lysates and CM from multiple macrophage-like cell lines, including Raw 264.7, THP1, and BV2. Importantly, low molecular mass immunoreactive species migrating between 14 and 16 kDa were readily detected in serum-free CM (Fig. 4*C, right panel*). These 14–16-kDa immunoreactive species corresponded to the size of the low molecular mass mAb XL313-reactive collagen fragments detected following MMP-mediated proteolytic digestion of purified collagen. To further study the XL313-immunoreactive species detected in macrophages, we examined the generation of the 14–16-kDa RGDKGE-containing XL313 fragments in Raw 264.7 macrophages. First, to examine the expression of collagen in these macrophages, we confirmed the expression of mRNA for the α1 and α2 chains of collagen type I in RAW macrophages by PCR (data not shown). Second, although we did not detect any full-length collagen type I in either cell lysates or CM from macrophages using anti-collagen type I-specific antibodies, we did detect low molecular mass fragments migrating at the same molecular mass as the RGDKGE-containing epitope in both cell lysates and CM using either mAb XL313 or an anti-collagen I-specific antibody (Fig. 4*D*). Importantly, shRNA-mediated knockdown of the α2 chain of collagen type I reduced immune detection of the low molecular mass species (14–16 kDa) in both lysates and CM when using either anti-collagen specific antibodies or mAb XL313 (Fig. 4*D*). When taken together, these findings are consistent with the possibility that macrophages are at least one cellular source of the RGDKGE collagen epitope.

Induction of Angiogenesis and Inflammation in Vivo by Soluble RGDKGE but Not a Related RGDAPG-containing Collagen Epitope—Given the differential expression and bio-distribution of the RGDKGE epitope in angiogenic CAM tissues and its expression in macrophage-conditioned medium, we examined whether a soluble circulating form of this RGDKGE epitope could be generated. To examine this possibility, chick embryos were either untreated or stimulated with FGF-2, and serum was collected 3 days later. As shown in Fig. 5*A*, low levels of circulating mAb XL313 immunoreactive epitope could be detected in the serum from non-stimulated control chick embryos. In contrast, a significant ($p < 0.05$) 2-fold increase was detected in the levels of circulating XL313 epitope following FGF-2 stimulation. Importantly, although the exact nature of the circulating XL313 epitope is not known, mAb XL313 demonstrated the ability to dose-dependently detect increasing levels of P-2 peptide representing the RGDKGE collagen epitope (data not shown), confirming the ability of the ELISA to dose-dependently detect the XL313 epitope. These findings suggest the differential detection of a soluble form of this RGDKGE-containing collagen epitope.

Given that a soluble form of the RGDKGE epitope could be detected *in vivo*, we next examined whether a soluble peptide containing the XL313 epitope might actively regulate angiogenesis and inflammation. To examine this possibility, we assessed the effects of the RGDKGE-containing collagen peptide on angiogenesis and inflammation in the chick CAM. As shown in Fig. 5*B*, the XL313 RGDKGE-containing collagen peptide (P-2) dose-dependently enhanced angiogenesis with maximum induction observed at a dose of 100 ng/CAM. Stimulation of CAMs with the RGDKGE-containing collagen peptide P-2, but not the related RGDAPG-containing collagen peptide P-1 or P-C, significantly ($p > 0.05$) induced angiogenesis as compared with no treatment (Fig. 5*C*).

Previously published studies implicate inflammation as a contributing factor in regulating angiogenesis (37, 39). Therefore, we also examined the effects of the soluble RGD-containing collagen peptides on inflammation. As shown in Fig. 5*D*, FGF-2 induced a strong inflammatory response in the chick CAM in the absence of CA as indicated by ~55–60% of the CAMs exhibiting extensive tissue thickening. Interestingly, minimal evidence of tissue inflammation was observed following stimulation with either P-C or the RGDAPG-containing collagen peptide P-1, although the RGDKGE collagen peptide P-2 significantly ($p < 0.05$) induced inflammation to nearly that of FGF-2 stimulation (Fig. 5*D*). Given that collagen peptide P-4 contains the identical RGDKGE sequence within its C-terminal region, but is different from that of P-2 in that it contains an isoleucine at the 3rd amino acid position instead of a proline

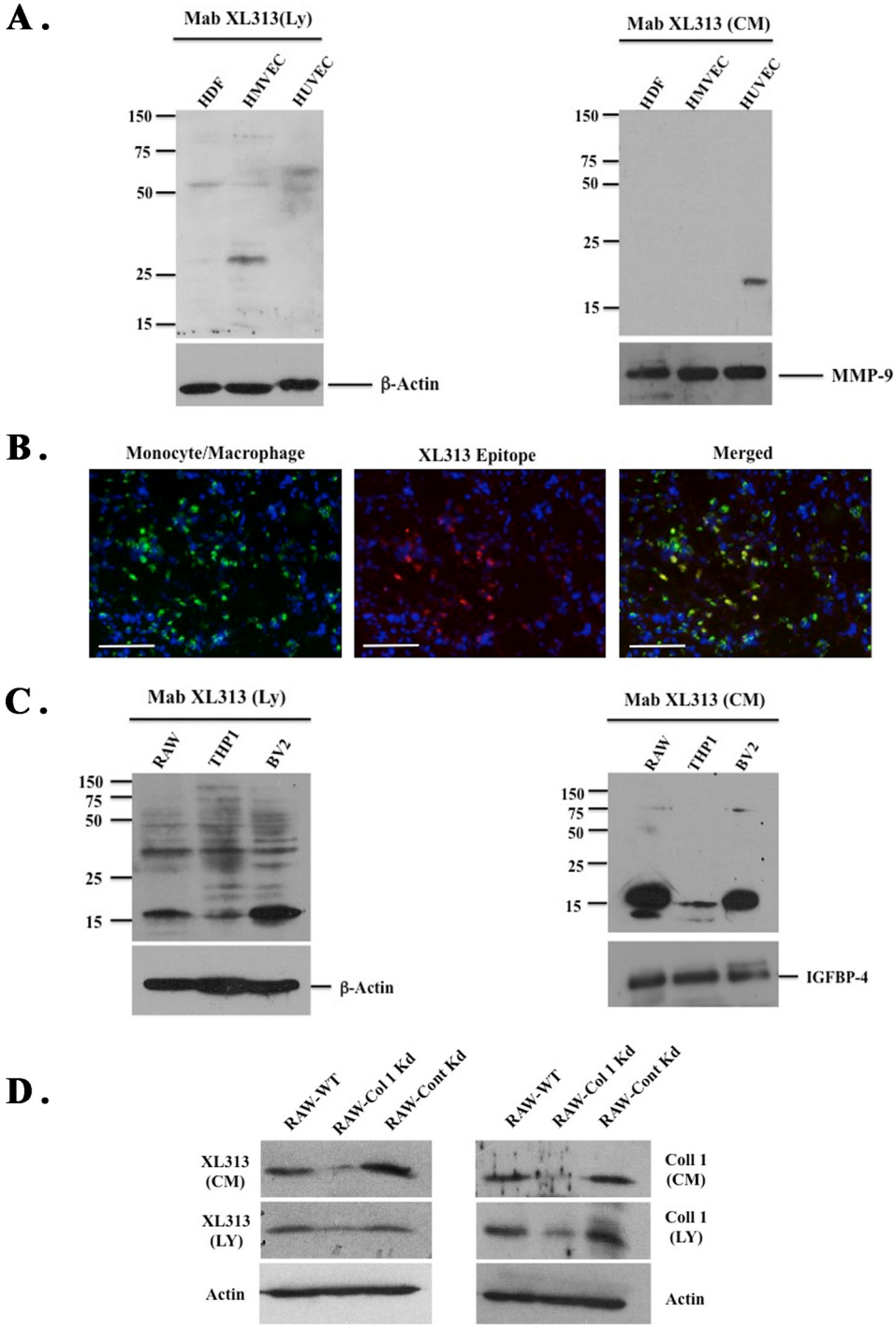

FIGURE 4. **Generation of XL313 cryptic RGDKGE epitope.** *A,* Western blot of whole cell lysates (*left panel*) or serum-free conditioned medium (*right panel*) from stromal cells probed with mAb XL313 or loading control antibodies for β-actin or MMP-9. *B,* representative examples of FGF-2-stimulated CAM tissues co-stained for expression of avian macrophages (*green*) and the RGDKGE-containing epitope (*red*). *Scale bars,* 50 μm. *C,* Western blot of whole cell lysates (*left panel*) or serum-free conditioned medium (*right panel*) from macrophage cell lines probed with mAb XL313 or loading control antibodies for β-actin or IGFBP-4. *D,* Western blot of whole cell lysates or serum-free conditioned medium from RAW 264.7 macrophage cells that were either not transfected (*WT*) or transfected with α2(I) specific shRNA (*Col 1 Kd*) or control nonspecific shRNA (*Cont Kd*) with mAb XL313 (*left panel*) or anti-collagen-1 antibody (*right panel*).

present in P-2, we compared the ability of these collagen peptides to stimulate inflammation. As shown in Fig. 5, *E* and *F*, peptides P-2 and P-4 containing the RGDKGE motif, showed no statistically significant difference in ability to induce CAM inflammation. Interestingly, although FGF-2 stimulated CAM tissues exhibited significantly ($p < 0.05$) higher relative levels of macrophages than either P-2 or P-4, no difference in the relative levels of macrophages was detected between P-2 and P-4 (data not shown). Collectively, these studies suggest that the biological impact of RGD-containing collagen peptides on angiogenesis and inflammation in the chick CAM may depend in part on their associated flanking sequences.

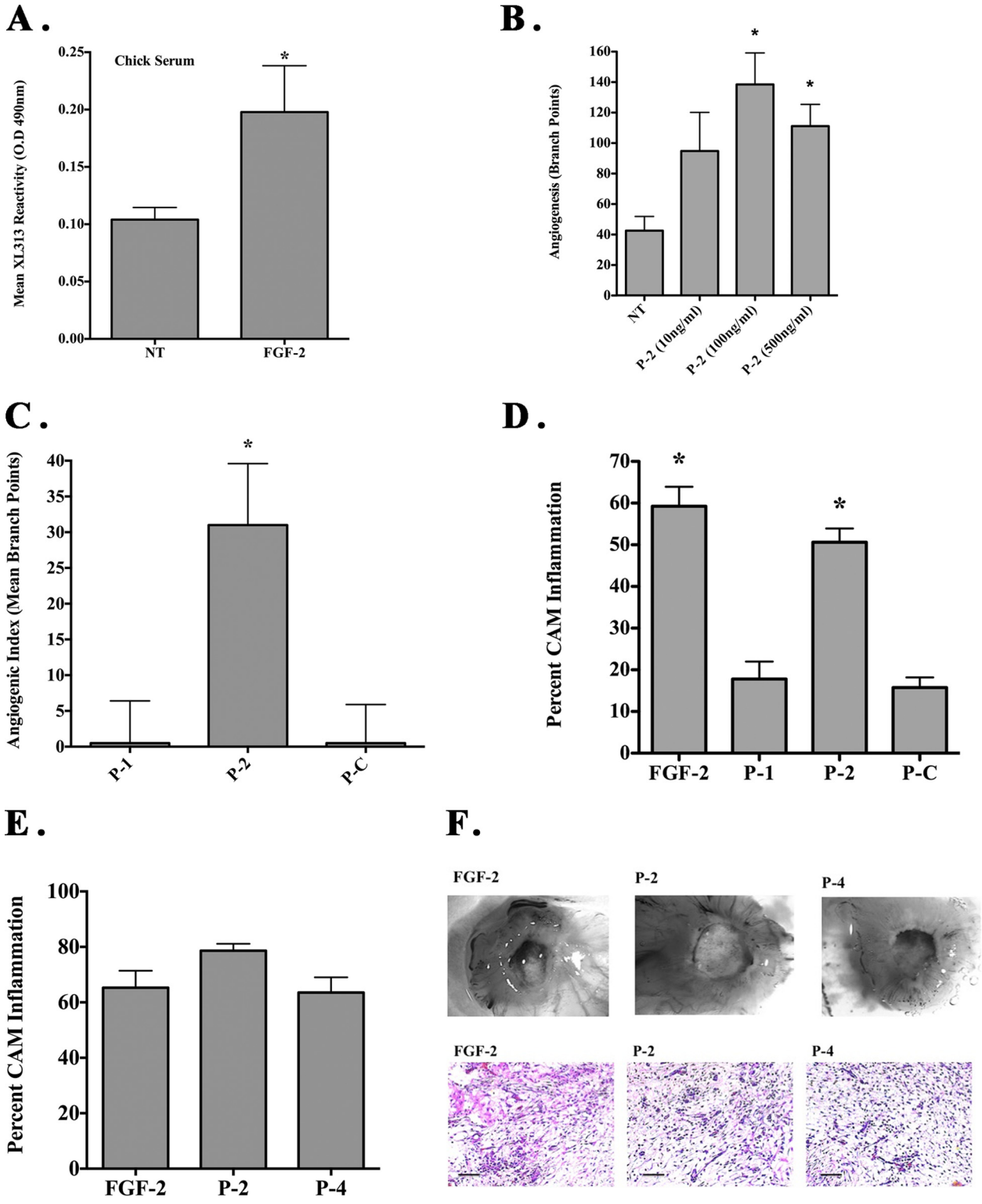

FIGURE 5. **Induction of angiogenesis and inflammation *in vivo* by soluble RGDKGE but not a related RGDAPG-containing collagen epitope.** *A,* serum from chick embryos in which the CAMs had been either not stimulated (*NT*) or stimulated with FGF-2 was collected. Relative levels of circulating mAb XL313-reactive epitope were quantified by solid phase ELISA. *Data bars* represent mean mAb XL313 reactivity ± S.E. (n = 12–13). *B,* quantification of dose-dependent induction of angiogenesis by RGDKGE-containing collagen peptide P-2. *Data bars* indicate mean number of branch points ± S.E. from 8 to 12 animal per condition. *C,* quantification of CAM angiogenesis associated with RGD-containing collagen peptides P-1 (KGDRGDAPG), P-2 (QGPRGDKGE), or control peptide P-C (QGPSGSPGE). *Data bars* indicate mean angiogenic index derived by subtracting the number of branch points from non-stimulated CAMs ± S.E. from 8 to 12 animals per condition. *D,* quantification of CAM inflammation associated with FGF-2, RGD-containing collagen peptides P-1 (KGDRGDAPG), P-2 (QGPRGDKGE), or control peptide P-C (QGPSGSPGE). *E,* quantification of CAM inflammation associated with FGF-2, RGD-containing collagen peptides P-2 (QGPRGDKGE), or P-4 (QGIRGDKGE). All experiments were conducted at least three times with similar results. *, $p < 0.05$. *F,* representative examples of inflammatory CAM thickening (×40) (*top panel*), or Giemsa-positive inflammatory infiltrates (×200) (*bottom panel*) from CAM inflammation associated with FGF-2, peptides P-2 (QGPRGDKGE), or P-4 (QGIRGDKGE). *Scale bars,* 50 μm.

RGDKGE-containing Peptide P-2-induced Angiogenesis Depends on p38 MAPK—Studies have indicated that angiogenesis and inflammation in the chick CAM is associated with alterations in MAPK signaling, including p38 MAPK (40, 41). To examine mechanisms that may regulate angiogenesis following stimulation with the RGDKGE-containing collagen peptide P-2, we examined CAM tissues from untreated or RGD peptide-treated animals. As shown in Fig. 6*A*, elevated levels of phosphorylated p38 MAPK were detected in lysates from CAMs treated with RGDKGE-containing peptide P-2 as compared with either untreated or RGDAPG-containing peptide P-1-treated animals. Quantification of CAM tissues (n = 12)

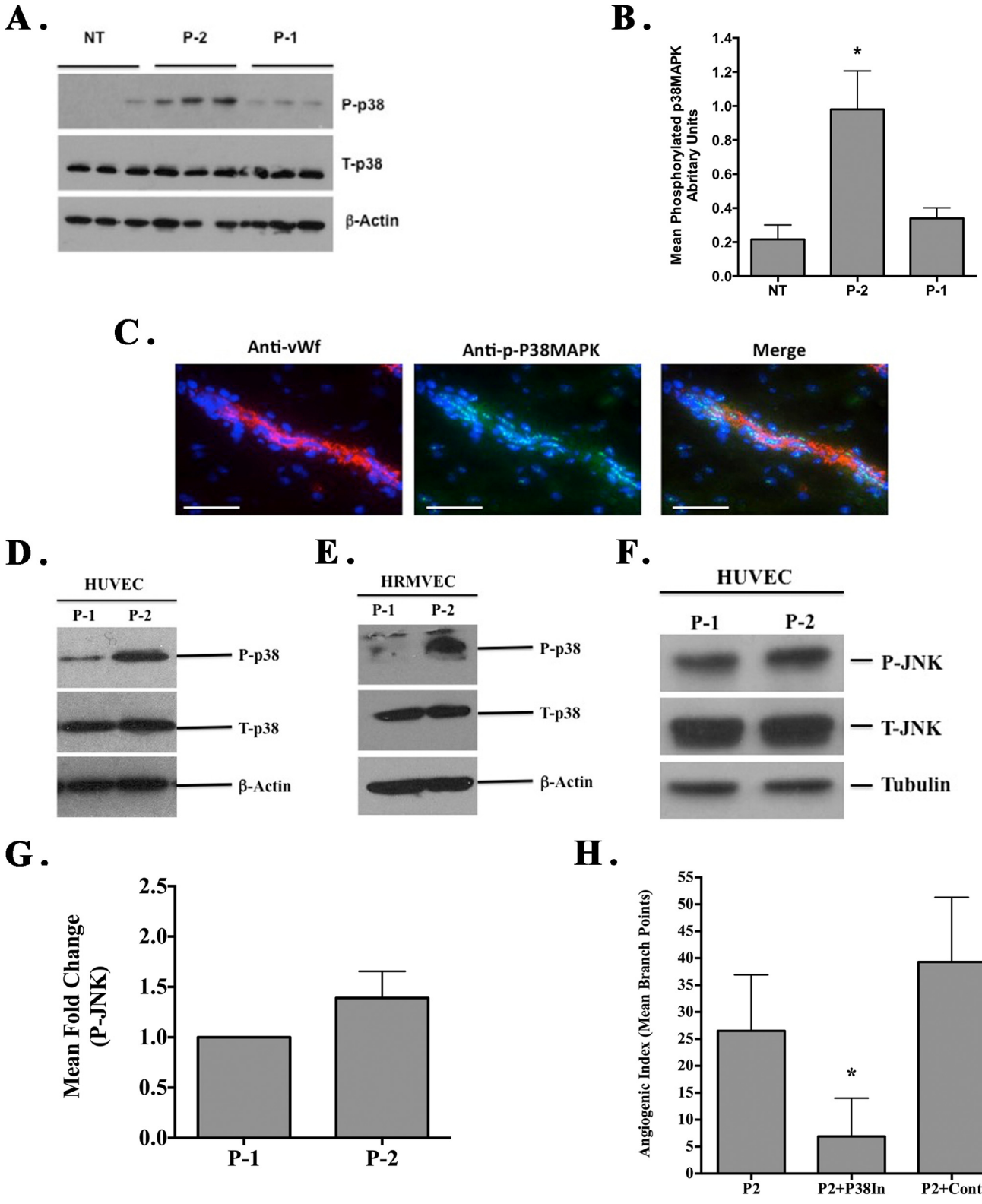

indicated a significant ($p < 0.05$) ~4-fold increase in phosphorylation of p38 MAPK as compared with controls (Fig. 6*B*). Consistent with our previous studies (41), although activated p38 MAPK could be detected in multiple cell types in chick CAMs, co-staining analysis indicated expression of phosphorylated p38 MAPK in vWf-positive blood vessels (Fig. 6*C*). Given these findings we examined the effects of the RGD-containing collagen peptides on the levels of phosphorylated p38 MAPK in endothelial cells. As shown in Fig. 6, *D* and *E*, whereas both RGD-containing collagen peptides P-1 and P-2 can support cell binding, interactions with RGDKGE collagen peptide P-2 resulted in enhanced phosphorylation of p38 MAPK as compared with RGDAPG collagen peptide P-1 in HUVECs (*left panel*) or HRMVEC (*right panel*). In similar studies, whereas a small increase (1.39-fold) in the phosphorylation of JNK was detected in HUVECS following interactions with P-2 as compared with P-1, this increase did not meet statistical significance (Fig. 6, *F* and *G*). Importantly, a functional role for p38 MAPK in mediating RGDKGE peptide P-2-induced angiogenesis *in vivo* was demonstrated, as P-2-induced angiogenesis was significantly ($p < 0.05$) reduced by a p38 MAPK inhibitor (Fig. 6*H*). Taken together, these data are consistent with a role for p38 MAPK in the peptide P-2-stimulated pro-angiogenic response observed *in vivo*.

Collagen Peptide P-2 Binds and Activates αvβ3 and Stimulates p38 MAPK Activation in an Src-dependent Manner—It is well established that multiple integrins can recognize RGD amino acid motifs within ECM proteins. However, the ability of an integrin to bind distinct RGD epitopes depends in part on its orientation within the parent molecule and the C-terminal amino acid sequences flanking the RGD motif (25–27). Given our observations, we sought to identify potential cell surface receptors that mediate interactions with the RGDKGE, containing collagen P-2 peptide. We examined the ability of endothelial cells to bind the RGD collagen peptides P-1 and P-2 in the presence or absence of function-blocking anti-integrin antibodies. As shown in Fig. 7*A*, anti-β1-specific antibody had little effect on HUVEC adhesion to peptide P-2, whereas anti-αvβ3 antibody significantly ($p < 0.05$) inhibited interactions by ~90% as compared with control. Anti-αvβ5 antibody showed little inhibition. Similar results were observed with P-1, which contains the RGDAPG sequence (Fig. 7*B*). These data suggest that αvβ3 can function as a receptor for both RGD-containing peptides in endothelial cells.

Given the ability of both RGD-containing peptides to bind αvβ3 coupled with the differential effect of these peptides on angiogenesis and inflammation, we sought to determine whether the RGD peptides differentially altered αvβ3-mediated signaling. Endothelial cells were allowed to attach to P-1 and P-2, and the relative level of β3-integrin phosphorylation was examined. As shown in Fig. 7*C*, in the absence of any growth factors, β3 phosphorylation was significantly ($p < 0.05$) increased by over 3-fold following ligation of RGDKGE peptide P-2 as compared with RGDAPG peptide P-1. Ligand binding of β3-integrin can induce receptor clustering and initiate downstream signaling events, including activation of protein kinases such as Fak and Src (42). Therefore, we assessed the differential phosphorylation of these protein kinases following the early mechanically mediated interactions with the RGD-containing collagen peptides. Little if any Fak phosphorylation was detected following ligation of either P-1 or P-2 under these serum-free conditions (data not shown). In contrast, Src phosphorylation was enhanced by nearly 2-fold following interactions with P-2 as compared with P-1 (Fig. 7*D*). Moreover, activation of β3-integrin and p38 MAPK in endothelial cells following binding to P-2 was dependent on Src as incubation of endothelial cells with an Src inhibitor reduced β3 and p38 MAPK phosphorylation in cells attached to collagen peptide P-2 (Fig. 7, *E* and *F*). Activation of Src and p38 MAPK can lead to enhanced actin polymerization and stress fiber formation (43–45); therefore, we examined the actin cytoskeleton in endothelial cells following binding to the RGD collagen peptides. Interestingly, endothelial cell interactions with the RGDKGE collagen peptide P-2 resulted in accelerated actin stress fiber formation as a statistically significant increase in the percentage of cells with actin stress fibers were observed in endothelial cells attached to P-2 (RGDKGE) as compared with interactions with P-1 (RGDAPG) peptide (Fig. 7, *G* and *H*). Given the ability of integrin αvβ3 to bind both the RGD-containing collagen peptides P-1 and P-2, we examined expression of αvβ3-integrin in endothelial cells attached to these RGD peptides (data not shown). Although some variation in distribution of αvβ3 was observed between cells exhibiting a more spread morphology, relatively little difference could be detected in the relative localization of αvβ3 between cells attached to P-1 and P-2 (data not shown). Taken together, these findings are consistent with the ability of the conserved RGDKGE collagen epitope to stimulate initiation of a β3-integrin-dependent mechano-transduction pathway.

Cellular Interactions with RGDKGE-containing Peptide Enhances Nuclear YAP Accumulation and Endothelial Cell Growth—Our data indicate that although both RGD-containing collagen peptides P-1 and P-2 can support an initial β3-in-

FIGURE 6. **RGDKGE-containing collagen peptide P-2-induced angiogenesis depends on p38 MAPK.** Angiogenesis was induced within the chick CAMs, and the relative level of p38 MAPK was assessed. *A,* Western blot of examples ($n = 3$ per condition) of total lysate from unstimulated (*NT*) or CAMs stimulated with P-1 (KGDRGDAPG) or P-2 (QGPRGDKGE) and probed for phosphorylated p38 MAPK (*P-p38*), total p38 MAPK (*T-p38*), or β-actin. *B,* quantification (ImageJ) of the mean relative levels of phosphorylated p38 MAPK from unstimulated or following CAM stimulation with P-1 (KGDRGDAPG) or P-2 (QGPRGDKGE). *Data bars* represent mean levels of phosphorylated p38 MAPK ± S.D. ($n = 8$–10 CAMs per condition). *C,* representative examples of P-2 stimulated CAM tissues co-stained for expression of vWf and phosphorylated p38 MAPK. *Scale bar,* 50.0 μm. *D,* Western blot analysis of endothelial cell (*HUVEC*) lysates from cells attached to collagen peptides P-1 (KGDRGDAPG) or P-2 (QGPRGDKGE) and probed for phosphorylated p38 MAPK (*P-p38*), total p38 MAPK (*T-p38*), or β-actin. *E,* Western blot analysis of endothelial cell (*HRMVEC*) lysates from cells attached to collagen peptides P-1 (KGDRGDAPG) or P-2 (QGPRGDKGE) and probed for phosphorylated p38 MAPK (*P-p38*), total p38 MAPK (*T-p38*), or β-actin. *F,* endothelial cells (*HUVEC*) were allowed to attach to either RGD-containing collagen peptides P-1 or P-2 for 15 min, and whole cells lysates were prepared. Western blot analysis of the expression of total (*T-JNK*) and phosphorylated (*P-JNK*) JNK or control tubulin. *G,* quantification of the mean relative levels of phosphorylated JNK following ImageJ analysis. *Data bars* represent mean fold change ± S.E. from four independent experiments with the relative levels of phosphorylated JNK with cells attached to P-1 set at 1.0. *H,* quantification of collagen peptide P-2 (QGPRGDKGE)-induced angiogenesis in the chick CAM following treatment with p38 MAPK inhibitor (*P38IN*) of DMSO control (*Cont*). *Data bars* represent angiogenic vessel branch points ± S.E. ($n = 8$–12 per condition). Experiments were conducted at least three times with similar results. *, $p < 0.05$.

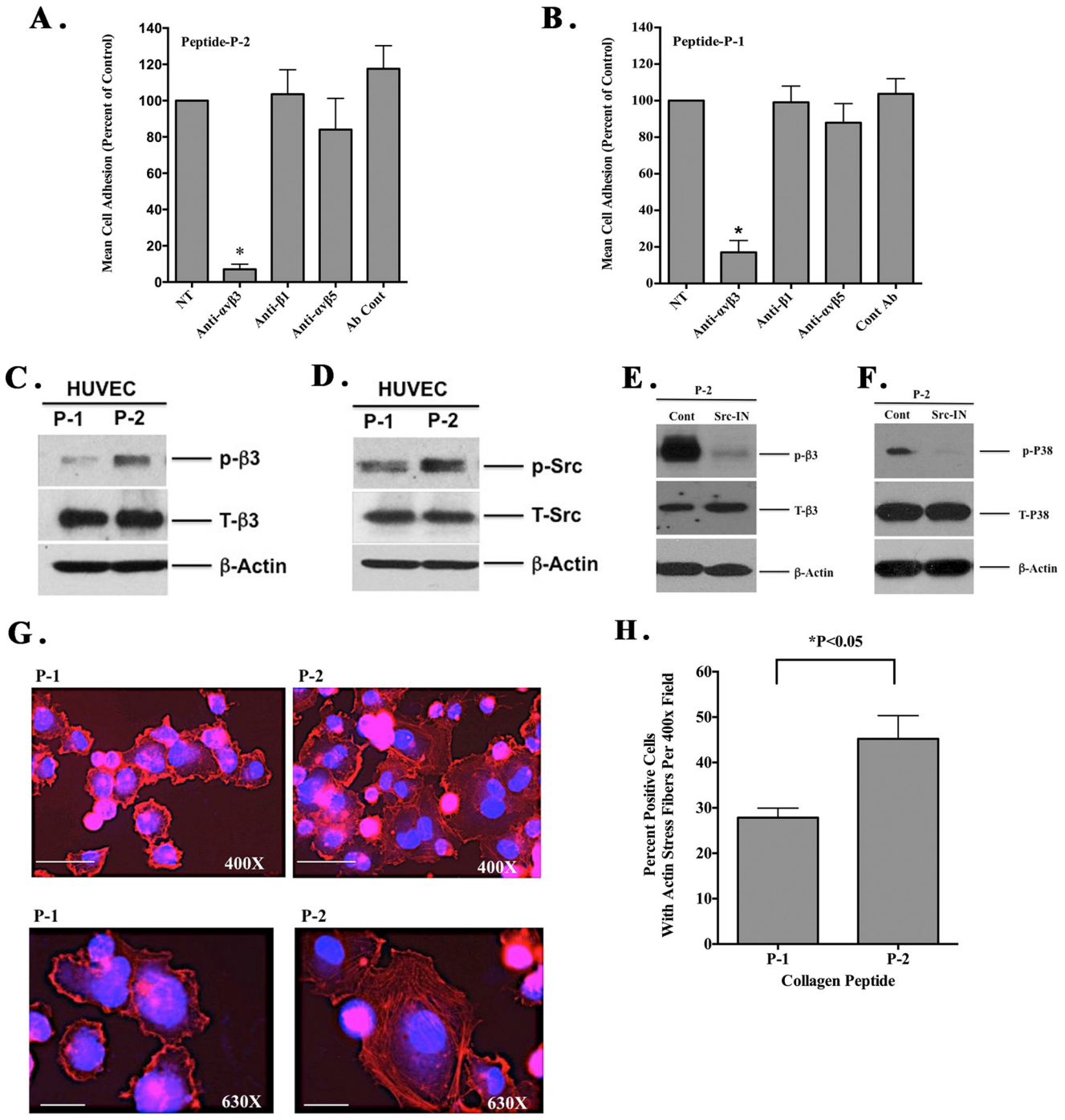

FIGURE 7. **Collagen peptide P-2 binds and activates $\alpha v\beta 3$ and stimulates p38 MAPK activation in an Src-dependent manner.** *A* and *B*, endothelial cells (HUVECS) were allowed to bind to wells coated with either RGDKGE-containing collagen peptide P-2 (*A*) or RGDAPG-containing collagen peptide P-1 (*B*) in the presence or absence of function-blocking anti-integrin antibodies. *Data bars* represent mean cell adhesion (±S.E. from four experiments). *, $p < 0.05$. *C*, Western blot of HUVEC lysates following binding to RGD-containing collagen peptides P-1 or P-2 probed with anti-phosphorylated β3-integrin (*p-β3*), total β3-integrin (*T-β3*), or β-actin. *D*, Western blot of HUVEC lysates following binding to RGD-containing collagen peptides P-1 or P-2 probed with anti-phosphorylated Src (*P-Src*), total Src (*T-Src*), or β-actin. *E*, Western blot of lysates prepared from HUVECs incubated in the presence or absence of an Src inhibitor PP2 (*Src-IN*) or control DMSO (*cont*) following binding to RGD-containing collagen peptides P-1 or P-2 probed with anti-phosphorylated β3-integrin (*p-β3*), total β3-integrin (*T-β3*) or β-actin. *F*, Western blot of lysates prepared from HUVECs incubated in the presence or absence of a Src inhibitor PP2 (*Src-IN*) or control DMSO (*cont*) following binding to RGD-containing collagen peptides P-1 or P-2 probed with anti-phosphorylated p38 MAPK (*p-P38*), total p38 MAPK (*T-P38*), or β-actin. *G*, representative examples of endothelial cells (HUVECs) attached to RGD containing collagen peptides P-1 and P-2 stained for F-actin. *Scale bar*, 25 μm. *H*, quantification of the mean percentage of HUVECs exhibiting actin stress fibers per ×400 field. *Data bars* represent mean counts from three independent experiments with 25 fields per condition. *, $p < 0.05$.

tegrin-mediated endothelial cell adhesive interaction, collagen peptide P-2 selectively enhanced β3-integrin phosphorylation leading to increased activation of p38 MAPK and accelerated actin stress fiber formation. Actin stress fiber formation and enhanced mechanical tension may contribute to re-localization of the transcriptional co-activator YAP to the nucleus (46). Moreover, YAP has recently been implicated in regulating angiogenesis and endothelial cell growth (47, 48). We examined

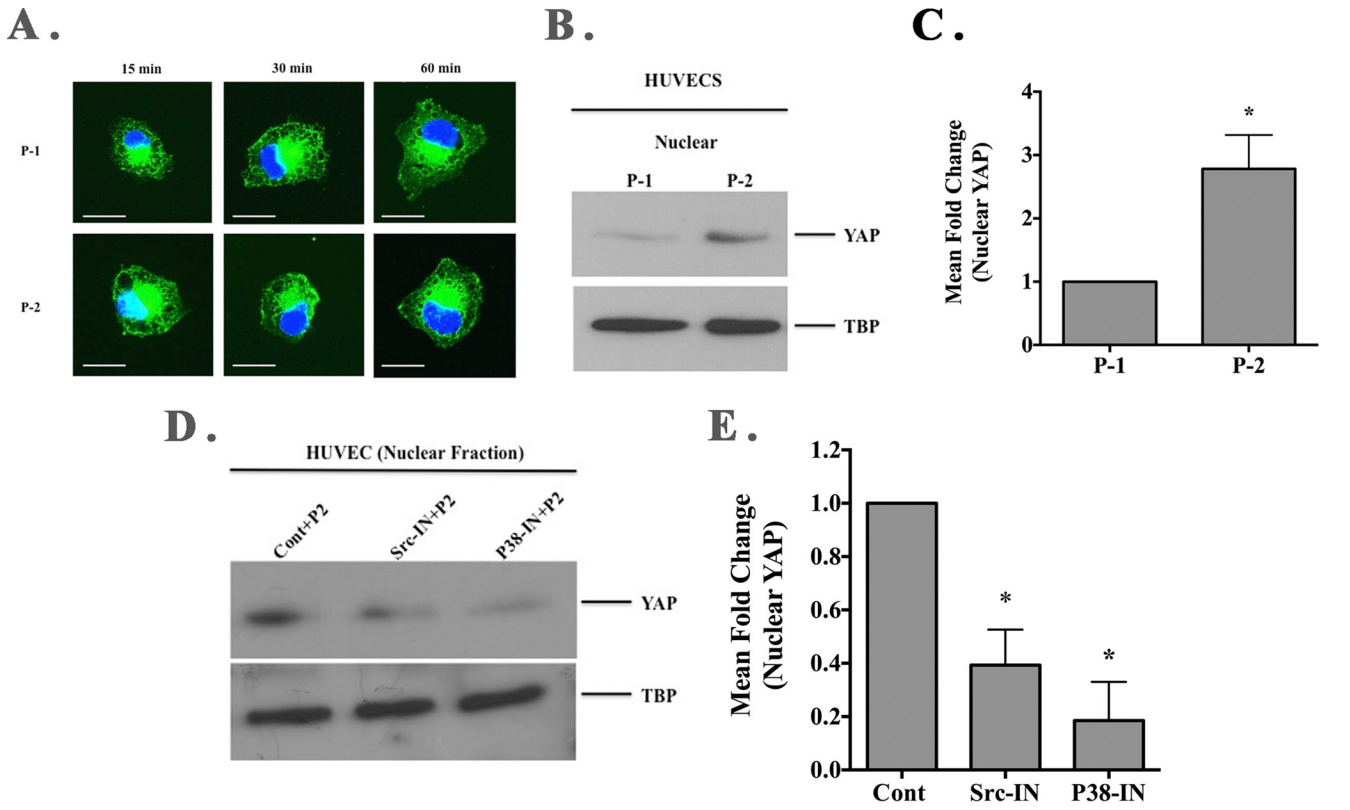

FIGURE 8. **Cellular interactions with RGDKGE collagen-containing peptide facilitates nuclear YAP accumulation.** *A,* representative examples of endothelial cells (*HUVECs*) attached to RGD-containing collagen peptides P-1 and P-2 stained for YAP (*green*). *Scale bar,* 50.0 μm. Photos were taken in a single plane at a magnification of $\times$630. *B,* Western blot of nuclear fraction of HUVEC lysates following binding to RGD-containing collagen peptides P-1 or P-2 probed with anti-YAP and anti-TATA-binding protein (*TBP*). *C,* quantification of the mean relative levels of nuclear YAP following ImageJ analysis. *Data bars* represent mean fold change $\pm$ S.E. from four independent experiments with the relative levels of nuclear YAP in cells attached to P-1 set at 1.0. *D,* Western blot of isolated nuclear fractions from cell lysates of endothelial cells (*HUVEC*) pre-incubated with Src or p38 MAPK inhibitor and stimulation with soluble RGD-containing collagen peptide P-2 and probed with YAP or TATA-binding protein (*TBP*). *E,* quantification of the mean relative levels of nuclear YAP following ImageJ analysis in cells attached to P-2 and pre-incubated with Src or p38 MAPK inhibitor. *Data bars* represent mean fold change $\pm$ S.E. from 2 to 3 independent experiments with the relative levels of nuclear YAP in cells under each condition with control (DMSO-treated) set at 1.0.

YAP localization following endothelial cell binding to the distinct collagen RGD-containing peptides in the absence of growth factor stimulation. As shown in Fig. 8*A*, enhanced level of nuclearly localized YAP was detected by 15 min following endothelial cell binding to collagen peptide P-2 as compared with P-1. The differential nuclear localization of YAP was not consistently detected at later times points, likely due to the lack of serum or growth factors during the time course of binding (49). To confirm and quantify the enhanced nuclear accumulation of YAP, Western blot analysis was carried out. As shown in Fig. 8*B*, the level of nuclear YAP was increased in endothelial cells attached to peptide P-2 as compared with peptide P-1. Quantification of four independent experiments indicated a significant ($p < 0.05$) 2.7-fold increase in the relative levels of nuclear YAP in endothelial cells attached to P-2 as compared with P-1 (Fig. 8*C*). Given the selective ability of P-2 to enhance Src-dependent activation of p38 MAPK, we examined whether the enhanced nuclear accumulation of YAP following RGDKGE peptide P-2 stimulation was Src- and/or p38 MAPK-dependent. As shown in Fig. 8*D*, nuclear YAP accumulation following P-2-stimulated endothelial cells was reduced by treatment with either Src or p38 MAPK inhibitors as compared with control. Quantification of 2–3 independent experiments indicated a 60–80% reduction in the relative levels of nuclear YAP in endothelial cells attached to P-2 following treatment with either Src or P38 inhibitors (Fig. 8*E*). These findings are consistent with a role for Src and p38 MAPK in mediating the RGDKGE P-2-stimulated nuclear accumulation of YAP.

YAP Contributes to P-2-stimulated Endothelial Cell Growth—Nuclear localization of YAP can contribute to the regulation of endothelial cell growth (47). Moreover, YAP has been shown to play a functional role in regulating angiogenesis (48, 49) and compounds known to inhibit YAP inhibit angiogenesis in the chick CAM model (50, 51). To this end, we identified an siRNA capable of significantly reducing the relative levels of YAP following *in vivo* transfection of CAM tissues (Fig. 9*A*). Consistent with these studies suggesting a role for YAP in regulating angiogenesis in the chick CAM, siRNA-mediated knockdown of YAP within the chick CAM significantly reduced FGF-2-induced angiogenesis (Fig. 9*B*).

Next, we examined the effects of RGD-containing collagen peptides on HUVEC and HRMVEC growth. Addition of soluble P-2 significantly ($p < 0.05$) enhanced endothelial cell growth, although stimulation with RGDAPG peptide P-1 had minimal if any effect (Fig. 9, *C* and *D*). YAP is thought to play roles in regulating the expression of multiple angiogenesis and inflammatory factors (47–49, 51); therefore, we examined whether P-2-stimulated endothelial cell growth might depend on YAP.

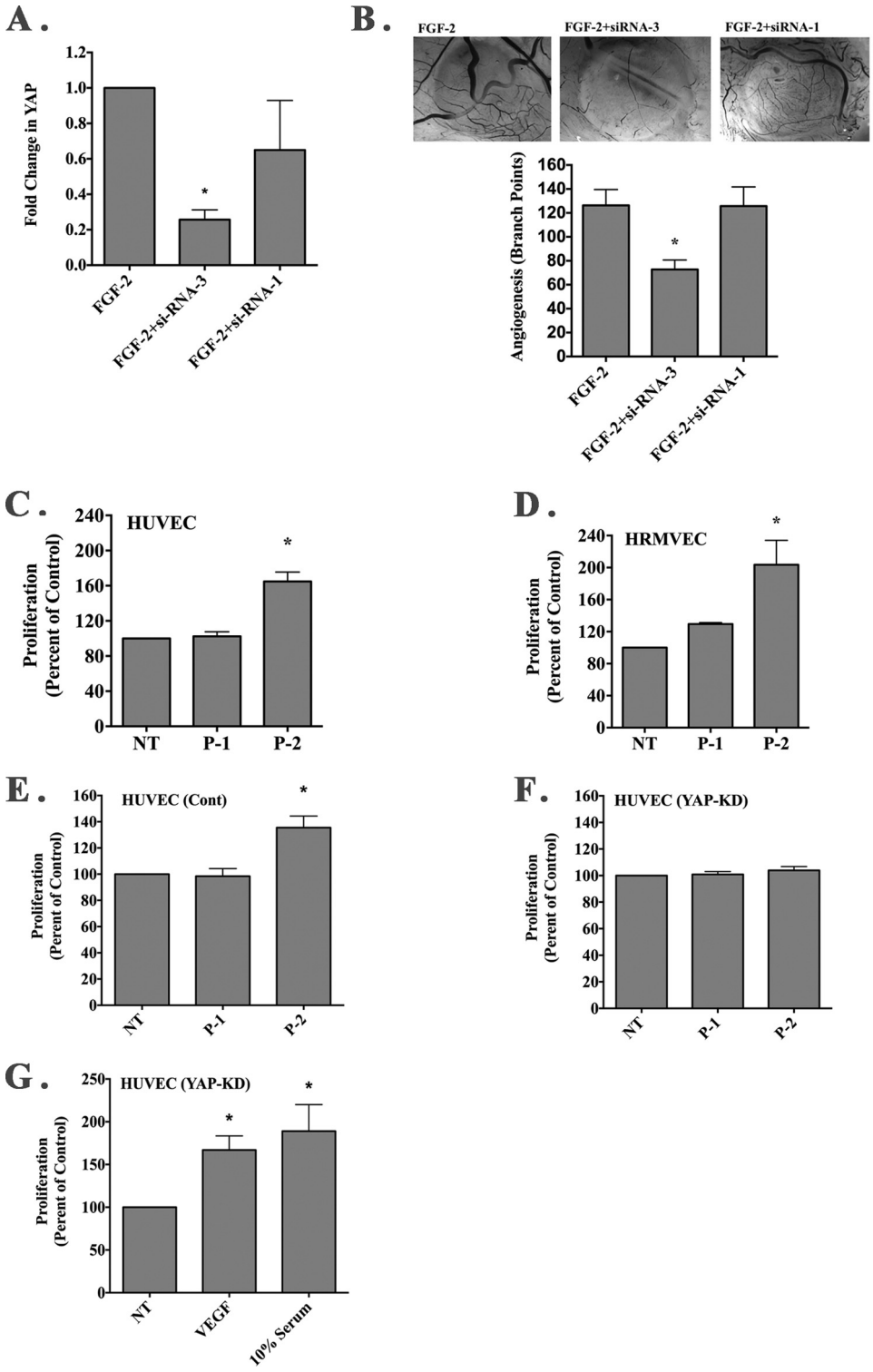

FIGURE 9. **YAP contributes to P-2-stimulated endothelial cell growth.** *A,* siRNAs directed to avian YAP were screened for their ability to knock down expression of YAP following *in vivo* transfection within FGF-2-induced CAM tissues by quantitative PCR. *Data bars* represent mean fold change in relative YAP levels ± S.E. from each condition. *, $p < 0.05$. *B,* representative examples of angiogenic CAM tissues from each condition (*top panel*). Photos were taken at a magnification of ×40. Quantification of the number of branching blood vessels from each condition (*bottom panel*). *Data bars* represent mean blood vessel branch point counts ± S.E. from 6 to 8 CAMs per conditions. *, $p < 0.05$. *C* and *D,* quantification of HUVEC (*C*) and HRMVEC (*D*) growth in the presence or absence of exogenously added RGD containing peptides P-1 or P-2. *Data bars* represent mean endothelial cell growth (±S.E.) from 3 to 4 independent experiments expressed as percent of control. *E* and *F,* quantification of endothelial cell growth in the presence or absence of exogenously added RGD-containing peptides P-1 or P-2 of cells transduced with nonspecific shRNA (*E*) or YAP-specific shRNA (*F*). *Data bars* represent mean endothelial cell growth (±S.E.) from four independent experiments. *G,* quantification of endothelial cell growth in the presence or absence of exogenously added VEGF (50 ng/ml) or 10% serum from cells transduced with YAP-specific shRNA. *Data bars* represent mean endothelial cell growth (±S.E.) from four independent experiments. *, $p < 0.05$.

To facilitate these studies, we transduced endothelial cells with YAP-specific or nonspecific shRNA. Addition of soluble RGDKGE-containing collagen peptide P-2 to endothelial cells, but not the related RGDAPG-containing peptide P1, significantly ($p < 0.05$) enhanced growth in control transduced cells (Fig. 9*E*), although the RGDKGE peptide P-2 failed to induce growth in endothelial cells in which YAP was knocked down (Fig. 9*F*). Importantly, YAP knockdown cells were capable of proliferating as enhanced growth was observed following VEGF or high serum stimulation (Fig. 9*G*). Taken together, our findings are consistent with a mechanism by which RGDKGE-containing collagen peptide P-2 may initiate a unique mechano-signaling cascade leading to the activation of p38 MAPK in an Src-dependent manner that ultimately leads to nuclear YAP accumulation and enhanced endothelial cell growth.

Discussion

A wide array of alterations in the composition and biomechanical properties of ECM proteins is known to occur during angiogenesis, and studies are beginning to define how these changes contribute to new blood vessel development (18, 21–23, 51, 53–55). Among the key cell surface molecules that play roles in mechano-transduction to facilitate information flow from outside the cell to the inside are integrin receptors. Integrins may act like information hubs by sensing diverse extracellular inputs and relaying this information into a complex network of intracellular circuits that ultimately modulate cellular behavior (4). The precise molecular mechanisms by which cells fine-tune their response to changes within the stromal microenvironment are not completely understood. Further complicating our understanding of new vessel development is the expanding number of cell types that contribute to tissue-specific control of angiogenesis such as distinct subsets of stromal fibroblasts, progenitor cells, and a variety of inflammatory cells such as neutrophils, mast cells, and macrophages. The roles played by these diverse cells during angiogenesis range from secretion of cytokines, chemokines, and proteolytic enzymes to the differential expression of other pro- and anti-angiogenic factors. Thus, tight control mechanisms must operate to allow coordination between these diverse compartments to govern tissue-specific vascular responses.

Among the most well studied integrins known to play a role in angiogenesis is $\alpha v\beta 3$. The complexity by which $\alpha v\beta 3$ regulates angiogenesis is illustrated by the fact that this receptor may exhibit both pro- and anti-angiogenic functions (7–15). Studies suggest that the distinct biological responses stimulated by binding to $\alpha v\beta 3$ may depend on many factors, including the mechanical and biochemical features of the particular ligands, the cell types within which $\alpha v\beta 3$ is expressed, as well as the concentration and manner by which the ligands are presented to the receptor (7–9, 24–27). For example, studies indicate that $\alpha v\beta 3$ binding to specific NC1 domains of collagen or selected RGD peptides can induce apoptosis, induce arteriole contraction, and inhibit angiogenesis (19, 29, 56), although other $\alpha v\beta 3$ ligands may promote cell survival, induce vascular dilation, and support angiogenesis (21–23, 30, 57). These observations are consistent with the notion that the final outcome of $\alpha v\beta 3$-mediated signaling may depend to a large extent on the particular characteristics of the ligand. Although a wealth of data has shown that RGD peptides can inhibit angiogenesis when administered exogenously, the approach of using a cyclic RGD peptide to control tumor growth failed to significantly impact glioblastoma progression and patient survival in late stage clinical testing (31). Interestingly, studies have indicated that specific RGD peptides may activate $\beta 3$-integrins (58, 59), and under-defined experimental conditions induce angiogenesis and tumor growth (30). These findings and other studies suggesting that amino acids C-terminal to the RGD motif play roles in governing integrin-selective binding prompted us to examine the biological significance of naturally occurring RGD-containing epitopes on angiogenesis.

Sequence analysis of RGD sites within collagen type I indicate that the KGE tri-peptide motif that is C-terminal to the RGD site was highly conserved among diverse species, although considerable variation is observed in the other collagen RGD-flanking sequences. Although all five of the collagen RGD epitopes can support cell binding, the highly conserved RGDKGE collagen peptide P-2 may play a functional role in angiogenesis and inflammation given that mAb XL313 directed to this epitope but not an antibody that recognizes the other three RGD collagen sites inhibited angiogenesis and inflammation *in vivo*. Although we cannot precisely differentiate between the three other naturally occurring non-RGDKGE-containing collagen epitopes, one or more of these epitopes were detected *in vivo* in addition to the RGDKGE epitope. Given that these RGD-containing epitopes are thought to be largely cryptic and not readily accessible to cell surface receptors, our findings are consistent with active collagen remodeling resulting in generation of neoepitopes during new vessel formation.

ECM remodeling occurs as an early event during angiogenesis and multiple proteolytic enzymes, including MMPs as well as serine and cysteine proteases that have the capacity to degrade intact or structurally altered forms of collagen (18, 60). Although our *in vitro* studies indicate that MMP-2-mediated degradation of collagen can lead to the generation of low molecular weights fragments recognized by mAb XL313, the precise mechanism by which the RGDKGE collagen epitope is generated *in vivo* is not completely understood. Analysis of angiogenic CAM tissues suggests that a subset of macrophages may be an important source of the RGDKGE epitope. Activated macrophages with M2-like characteristics can express multiple enzymes capable of degrading collagen and in turn can internalize and further degrade collagen into small low molecular weight fragments (35, 38). Although little evidence exists that macrophages generate and deposit intact triple helical collagen type I, studies have indicated that certain isoforms of collagen may be expressed (61). Consistent with previous reports, we did not detect intact collagen; however, we did detect low molecular weight RGDKGE-containing collagen fragments in both whole cell lysates and serum-free conditioned medium from macrophage-like cell lines. Although our studies do not rule out macrophage-mediated collagen internalization as a contributing factor to the *in vivo* generation of the RGDKGE collagen epitope, our *in vitro* studies were carried out in the absence of serum or exogenously added collagen, and thus are consistent

with the active generation of the RGDKGE collagen fragment by macrophages.

Activated macrophages, including M2-polarized macrophages, have been implicated in supporting angiogenesis and inflammation as multiple factors secreted by these cells exhibit pro-angiogenic activities (35, 62). Although many studies indicate that synthetic RGD-containing peptides inhibit angiogenesis and tumor growth, our findings provide the first evidence that macrophages may generate and release an RGDKGE-containing collagen epitope that may exhibit pro-angiogenic activity. Importantly, previous studies have suggested that certain RGD peptides can activate $\alpha v\beta 3$ (58, 59) and may enhance vascular permeability (45, 57), which might lead to release of inflammatory factors, which in turn may contribute to the formation of new blood vessels.

To examine possible mechanisms by which the RGDKGE collagen peptide might regulate angiogenesis, we first sought to identify endothelial cell receptors for this motif. Although we do not rule out the possibility that additional non-integrin receptors may bind this collagen epitope, our data suggest that $\alpha v\beta 3$ can function as an endothelial cell receptor for the RGDKGE motif. Interestingly, $\alpha v\beta 3$ bound both the RGDKGE and RGDAPG collagen peptides, yet only RGDKGE peptide significantly induced angiogenesis and inflammation *in vivo*. These findings are consistent with the notion that distinct RGD-containing $\alpha v\beta 3$ ligands may promote different biological responses. Signaling downstream from $\alpha v\beta 3$ is complex, and studies have indicated that simple binding of $\beta 3$-integrin does not necessarily lead to productive outside-in integrin signaling (63). In fact, the capacity of $\beta 3$-integrins to promote outside-in signaling depends on multiple factors, including the extent of receptor clustering and subsequent generation of mechanical tension within the actin cytoskeleton, recruitment of adaptor and accessory proteins such as Gα13 and Kindlin-2, and the association of the integrin with protein-tyrosine phosphatases and certain growth factor receptors (64–67). Although the exact mechanisms leading to RGDKGE-mediated $\alpha v\beta 3$ signaling is not completely understood, endothelial cell interactions with the RGDKGE peptide in the absence of serum led to enhanced phosphorylation of $\beta 3$-integrin on tyrosine 747 and of Src phosphorylation at tyrosine 416. These data and others are consistent with an early mechanically mediated activation of $\beta 3$-integrin that depends on Src given that blocking Src activity reduced $\beta 3$ phosphorylation following binding to the RGDKGE motif.

Integrin signaling and Src activation are known to regulate the architecture of the actin cytoskeleton (66–68). Moreover, Src family kinases regulate p38 MAPK, and activation of p38 MAPK is thought to enhance actin stress fiber formation in endothelial cells and regulate angiogenesis *in vivo* (39–45). Our findings provide new insight into the coordinated roles of p38 MAPK and Src in regulating RGD-dependent endothelial cell signaling through $\alpha v\beta 3$ as interactions with the RGDKGE cryptic collagen epitope leads to enhanced p38 MAPK phosphorylation in an Src-dependent manner. Moreover, RGDKGE-induced angiogenesis *in vivo* was associated with enhanced levels of phosphorylated p38 MAPK, and the angiogenic response was reduced by inhibiting p38 MAPK. These findings are consistent with the notion that RGDKGE-stimulated angiogenesis depends on p38 MAPK.

New studies have suggested a role for actin stress fibers and mechanical tension in promoting nuclear accumulation of YAP, where it is thought to function in conjunction with TEAD transcription factors in regulating gene expression (46–49, 52). Given data suggesting a role for YAP in regulating endothelial cell growth and angiogenesis, we examined the subcellular distribution of YAP in endothelial cells following interaction with the RGDKGE collagen peptide. Our data indicate that endothelial cell interaction with the RGDKGE epitope was associated with enhanced nuclear accumulation of YAP. Integrin signaling may play a role in the regulation of YAP as studies have implicated a role for $\beta 1$-integrins expressed in skeletal stem cells and αV-integrins expressed in osteoblasts in governing YAP subcellular localization (69, 70). Our findings are consistent with a mechanism by which $\alpha v\beta 3$-mediated binding to the RGDKGE epitope, but not the related RGDAPG epitope, stimulates a signaling cascade leading to enhanced nuclear accumulation of YAP that depends on Src and/or p38 MAPK. This possibility is supported by our findings that reduced level of nuclear YAP was detected following $\alpha v\beta 3$-mediated interaction with RGDKGE peptide in endothelial cells in which Src or p38 MAPK was inhibited. Given the documented role of YAP in governing cell growth coupled with the ability of the RGDKGE collagen peptide to stimulate nuclear accumulation of YAP and enhance endothelial cell growth, it is possible that the RGDKGE collagen peptide-induced endothelial cell growth is YAP-dependent. Consistent with this possibility, no enhancement of endothelial cell growth was detected following knockdown of YAP in endothelial cells stimulated with the RGDKGE collagen peptide, even though these cells are capable of proliferating as stimulation with VEGF or high levels of serum enhanced their growth. Given our studies, it would be interesting to speculate that part of the FGF-2-induced angiogenic response observed in the chick CAM model might involve the recruitment of macrophages that generate a previously uncharacterized RGDKGE-containing cryptic collagen epitope that binds to $\alpha v\beta 3$ leading to Src and p38 MAPK activation and nuclear accumulation of YAP. Given that YAP is known to regulate a wide array of genes that may impact angiogenesis and inflammation, including CTGF and Cyr61, it is likely that the RGDKGE collagen epitope may initiate a complex pro-angiogenic program *in vivo* involving YAP-associated regulation of multiple pro-angiogenic molecules and not simply be restricted to only enhancing endothelial cell growth.

Collectively, our studies provide new evidence that a highly conserved RGDKGE-containing collagen epitope can be generated by a subset of macrophages, and the RGDKGE collagen epitope can stimulate pro-inflammatory and angiogenic activity. Binding of the RGDKGE collagen epitope to $\beta 3$-integrin can initiate a signaling pathway in endothelial cells leading to activation of Src and p38 MAPK ultimately leading to nuclear accumulation of YAP and enhance cell growth. These novel studies provide new cellular and molecular insight into how an endogenously generated RGD-containing cryptic collagen epitope may promote rather that inhibit angiogenesis. Given the complexity of $\alpha v\beta 3$ functions and the growing body of evidence that

the final outcome of αvβ3 binding may depend on the nature of the particular ligand, our findings provide support for an alternative strategy to help control the biological activity of β3-integrin by specific targeting of endogenous pro-angiogenic ligands of αvβ3 rather than direct targeting of the receptor itself.

Author Contributions—J. J. A. conceived and coordinated studies, designed, performed, and analyzed experiments, and wrote the paper. L. C. coordinated studies and designed, performed, and analyzed experiments. J. M. C. coordinated the studies and designed, performed, and analyzed experiments. E. T. coordinated studies and performed and analyzed experiments. X. Y. coordinated studies and designed and performed experiments. R. F. coordinated studies, designed, and analyzed experiments. C. V. coordinated studies, designed, and analyzed experiments. P. C. B. conceived and coordinated the studies, designed, performed, and analyzed the experiments, and wrote the paper. All authors approved the final version of the manuscript.

References

1. Bergers, G., and Hanahan, D. (2008) Modes of resistance to anti-angiogenic therapy. *Nat. Rev. Cancer* **8,** 593–603
2. Chung, A. S., Lee, J., and Ferrara, N. (2010) Targeting the tumor vasculature: insight from physiological angiogenesis. *Nat. Rev. Cancer* **10,** 505–514
3. Cao, Y., Arbiser, J., D'Amato, R. J., D'Amore, P. A., Ingber, D. E., Kerbel, R., Klagsbrun, M., Lim, S., Moses, M. A., Zetter, B., Dvorak, H., and Langer, R. (2011) Forty-year journey of angiogenesis translational research. *Sci. Transl. Med.* **3,** 114rv3
4. Contois, L., Akalu, A., and Brooks, P. C. (2009) Integrins as functional hubs in the regulation of pathological angiogenesis. *Semin. Cancer Biol.* **19,** 318–328
5. Moserle, L., Jiménez-Valerio, G., and Casanovas, O. (2014) Antiangiogenic therapies: going beyond their limits. *Cancer Discov.* **4,** 31–41
6. Greenberg, J. I., Shields, D. J., Barillas, S. G., Acevedo, L. M., Murphy, E., Huang, J., Scheppke, L., Stockmann, C., Johnson, R. S., Angle, N., and Cheresh, D. A. (2008) A role for VEGF as a negative regulator of pericyte function and vessel maturation. *Nature* **456,** 809–813
7. Hodivala-Dilke, K. (2008) αvβ3 integrin and angiogenesis: a moody integrin in a changing environment. *Curr. Opin. Cell Biol.* **20,** 514–519
8. Atkinson, S. J., Ellison, T. S., Steri, V., Gould, E., and Robinson, S. D. (2014) Redefining the role(s) of endothelial αvβ3-integrin in angiogenesis. *Biochem. Soc. Trans.* **42,** 1590–1595
9. Robinson, S. D., and Hodivala-Dilke, K. M. (2011) The role of β3-integrins in tumor angiogenesis: context is everything. *Curr. Opin. Cell Biol.* **23,** 630–637
10. Brooks, P. C., Clark, R. A., and Cheresh, D. A. (1994) Requirement of vascular integrin αvβ3 for angiogenesis. *Science* **264,** 569–571
11. Brooks, P. C., Montgomery, A. M., Rosenfeld, M., Reisfeld, R. A., Hu, T., Klier, G., and Cheresh, D. A. (1994) Integrin αvβ3 antagonists promote tumor regression by inducing apoptosis of angiogenic blood vessels. *Cell* **79,** 1157–1164
12. Contois, L. W., Akalu, A., Caron, J. M., Tweedie, E., Cretu, A., Henderson, T., Liaw, L., Friesel, R., Vary, C., and Brooks, P. C. (2015) Inhibition of tumor-associated αvβ3 integrin regulates the angiogenic switch by enhancing expression of IGFBP-4 leading to reduced melanoma growth and angiogenesis *in vivo*. *Angiogenesis* **18,** 31–46
13. Reynolds, L. E., Wyder, L., Lively, J. C., Taverna, D., Robinson, S. D., Huang, X., Sheppard, D., Hynes, R. O., and Hodivala-Dilke, K. M. (2002) Enhanced pathological angiogenesis in mice lacking β3 integrin or β3 and β5 integrins. *Nat. Med.* **8,** 27–34
14. Feng, W., McCabe, N. P., Mahabeleshwar, G. H., Somanath, P. R., Phillips, D. R., and Byzova, T. (2008) The angiogenic response is dictated by β3 integrin on bone marrow-derived cells. *J. Cell Biol.* **183,** 1145–1157
15. Steri, V., Ellison, T. S., Gontarczyk, A. M., Weilbaecher, K., Schneider, J. G., Edwards, D., Fruttiger, M., Hodivala-Dilke, K. M., and Robinson, S. D. (2014) Acute depletion of endothelial β3-integrin transiently inhibits tumor growth and angiogenesis in mice. *Circ. Res.* **114,** 79–91
16. Gong, Y., Yang, X., He, Q., Gower, L., Prudovsky, I., Vary, C. P., Brooks, P. C., and Friesel, R. E. (2013) Sprouty4 regulates endothelial cell migration via modulating integrin β3 stability through c-Src. *Angiogenesis* **16,** 861–875
17. Adair-Kirk, T. L., and Senior, R. M. (2008) Fragments of extracellular matrix as mediators of inflammation. *Int. J. Biochem. Cell Biol.* **40,** 1101–1110
18. Davis, G. E. (2011) Angiogenesis and proteinases: influence on vascular morphogenesis, stabilization and regression. *Drug Discov. Today Dis. Models* **8,** 13–20
19. Petitclerc, E., Boutaud, A., Prestayko, A., Xu, J., Sado, Y., Ninomiya, Y., Sarras, M. P., Jr., Hudson, B. G., and Brooks, P. C. (2000) New functions for non-collagenous domains of human collagen type IV: novel integrin ligands inhibiting angiogenesis and tumor growth *in vivo*. *J. Biol. Chem.* **275,** 8051–8061
20. Sudhakar, A., Sugimoto, H., Yang, C., Lively, J., Zeisberg, M., and Kalluri, R. (2003) Human tumstatin and endostatin exhibit distinct antiangiogenic activities mediated by αvβ3 and α5β1 integrins. *Proc. Natl. Acad. Sci. U.S.A.* **100,** 4766–4771
21. Xu, J., Rodriguez, D., Petitclerc, E., Kim, J. J., Hangai, M., Moon, Y. S., Davis, G. E., Brooks, P. C., and Yuen, S. M. (2001) Proteolytic exposure of a cryptic site within collagen type IV is required for angiogenesis and tumor growth *in vivo*. *J. Cell Biol.* **154,** 1069–1079
22. Hangai, M., Kitaya, N., Xu, J., Chan, C. K., Kim, J. J., Werb, Z., Ryan, S. J., and Brooks, P. C. (2002) Matrix metalloproteinase-9-dependent exposure of a cryptic migratory control site in collagen is required before retinal angiogenesis. *Am. J. Pathol.* **161,** 1429–1437
23. Cretu, A., Roth, J. M., Caunt, M., Akalu, A., Policarpio, D., Formenti, S., Gagne, P., Liebes, L., and Brooks, P. C. (2007) Disruption of endothelial cell interactions with the novel HU177 cryptic collagen epitope inhibits angiogenesis. *Clin. Cancer Res.* **13,** 3068–3078
24. Pierschbacher, M. D., and Ruoslahti, E. (1987) Influence of stereochemistry of the sequence Arg-Gly-Asp-Xaa on binding specificity in cell adhesion. *J. Biol. Chem.* **262,** 17294–17298
25. Kunicki, T. J., Annis, D. S., and Felding-Haberman. (1997) Molecular determinants of Arg-Gly-Asp ligand specificity for β3 integrins. *J. Biol. Chem.* **272,** 4103–4107
26. Gurrath, M., Müller, G., Kessler, H., Aumailley, M., and Timpl. (1992) Conformational/activity studies of rationally designed potent anti-adhesive RGD peptides. *Eur. J. Biochem.* **210,** 911–921
27. Kostidis, S., Stavrakoudis, A., Biris, N., Tsoukatos, D., Sakarellos, C., and Tsikaris, V. (2004) The relative orientation of the Arg and Asp side chains defined by a pseudodihedral angle as a key criterion for evaluating the structure-activity relationship of RGD peptides. *J. Pept. Sci.* **10,** 494–509
28. Miyoshi, T., Hirohata, S., Ogawa, H., Doi, M., Obika, M., Yonezawa, T., Sado, Y., Kusachi, S., Kyo, S., Kondo, S., Shiratori, Y., Hudson, B. G., and Ninomiya, Y. (2006) Tumor-specific expression of the RGD-α3(IV)NC1 domain suppresses endothelial tube formation and tumor growth in mice. *FASEB J.* **11,** 1904–1906
29. Danhier, F., Le Breton, A., and Préat, V. (2012) RGD-based strategies to target α(v)β(3) integrin in cancer therapy and diagnosis. *Mol. Pharm.* **9,** 2961–2973
30. Reynolds, A. R., Hart, I. R., Watson, A. R., Welti, J. C., Silva, R. G., Robinson, S. D., Da Violante, G., Gourlaouen, M., Salih, M., Jones, M. C., Jones, D. T., Saunders, G., Kostourou, V., Perron-Sierra, F., Norman, J. C., *et al.* (2009) Stimulation of tumor growth and angiogenesis by low concentrations of RGD-mimetic integrin inhibitors. *Nat. Med.* **15,** 392–400
31. Stupp, R., Hegi, M. E., Gorlia, T., Erridge, S. C., Perry, J., Hong, Y.-K., Aldape, K. D., Lhermitte, B., Pietsch, T., Grujicic, D., Steinbach, J. P., Wick, W., Tarnawski, R., Nam, D.-H., Hau, P., *et al.* (2014) Cilengitide combined with standard treatment for patients with newly diagnosed glioblastoma with methylated MGMT promoter (CENTRIC EORTC 26071–22072 study): a multicenter, randomized, open-label, phase 3 trial. *Lancet* **15,** 1100–11008

32. Blasi, E., Barluzzi, R., Bocchini, V., Mazzolla, R., and Bistoni, F. (1990) Immortalization of murine microglial cells by a v-raf/v-myc carrying retrovirus. *J. Neuroimmunol.* **27,** 229–237
33. Rouslahti, E. (1996) RGD and other recognition sequences for integrins. *Annu. Rev. Cell Biol.* **12,** 697–715
34. Montgomery, A. M., Reisfeld, R. A., and Cheresh, D. A. (1994) Integrin αvβ3 rescues melanoma cells from apoptosis in three-dimensional dermal collagen. *Proc. Natl. Acad. Sci. U.S.A.* **91,** 8856–8860
35. Madsen, D. H., Leonard, D., Masedunskas, A., Moyer, A., Jürgensen, H. J., Peters, D. E., Amornphimoltham, P., Selvaraj, A., Yamada, S. S., Brenner, D. A., Burgdorf, S., Engelholm, L. H., Behrendt, N., Holmbeck, K., Weigert, R., and Bugge, T. H. (2013) M2-like macrophages are responsible for collagen degradation through a mannose receptor-mediated pathway. *J. Cell Biol.* **202,** 951–966
36. Zwadlo-Klarwasser, G., Görlitz, K., Hafemann, B., Klee, D., and Klosterhalfen, B. (2001) The chorioallantoic membrane of the chick embryo as a simple model for the study of the angiogenic and inflammatory response to biomaterials. *J. Mater. Sci. Mater. Med.* **12,** 195–199
37. Deryugina, E. I., and Quigley, J. P. (2008) Chick embryo chorioallantoic membrane models to quantify angiogenesis induced by inflammatory and tumor cells or purified effector molecules. *Methods Enzymol.* **444,** 21–41
38. Skjøt-Arkil, H., Barascuk, N., Register, T., and Karsdal, M. A. (2010) Macrophage-mediated proteolytic remodeling of the extracellular matrix in atherosclerosis results in neoepitopes: a potential new class of biochemical markers. *Assay Drug. Dev. Technol.* **8,** 542–552
39. Rajashekhar, G., Kamocka, M., Marin, A., Suckow, M. A., Wolter, W. R., Badve, S., Sanjeevaiah, A. R., Pumiglia, K., Rosen, E., and Clauss, M. (2011) Pro-inflammatory angiogenesis is mediated by p38 MAP kinase. *J. Cell. Physiol.* **226,** 800–808
40. Matsumoto, T., Turesson, I., Book, M., Gerwins, P., and Claesson-Welsh, L. (2002) p38 MAP kinase negatively regulates endothelial cell survival, proliferation, and differentiation in FGF-2 stimulated angiogenesis. *J. Cell Biol.* **156,** 149–160
41. Contois, L. W., Nugent, D. P., Caron, J. M., Cretu, A., Tweedie, E., Akalu, A., Liebes, L., Friesel, R., Rosen, C., Vary, C., and Brooks, P. C. (2012) Insulin-like growth factor binding protein-4 differentially inhibits growth factor-induced angiogenesis. *J. Biol. Chem.* **287,** 1779–1789
42. Mitra, S. K., and Schlaepfer, D. D. (2006) Integrin-regulated FAK-Src signaling in normal and cancer cells. *Curr. Opin. Cell Biol.* **18,** 516–523
43. McMullen, M., Keller, R., Sussman, M., and Pumiglia, K. (2004) Vascular endothelial growth factor-mediated activation of p38 is dependent upon Src and RAFTK/Pyk2. *Oncogene* **23,** 1275–1282
44. Rousseau, S., Houle, F., Landry, J., and Huot, J. (1997) p38 MAP kinase activation by vascular endothelial growth factor mediates actin reorganization and cell migration in human endothelial cells. *Oncogene* **15,** 2169–2177
45. Alghisi, G. C., Ponsonnet, L., and Ruegg, C. (2009) The integrin antagonist cilengitide activates αvβ3, disrupts VE-cadherin localization at cell junctions and enhances permeability in endothelial cells. *PLoS One* **4,** e4449
46. Dupont, S., Morsut, L., Aragona, M., Enzo, E., Giulitti, S., Cordenonsi, M., Zanconato, F., Le Digabel, J., Forcato, M., Bicciato, S., Elvassore, N., and Piccolo, S. (2011) Role of YAP/TAZ in mechanotransduction. *Nature* **474,** 179–183
47. Shen, Z., and Stanger, B. Z. (2015) YAP regulates S-phase entry in endothelial cells. *PLoS One* **10,** e0117522
48. Dai, X., She, P., Chi, F., Feng, Y., Liu, H., Jin, D., Zhao, Y., Guo, X., Jiang, D., Guan, K.-L., Zhong, T. P., and Zhao, B. (2013) Phosphorylation of angiomotin by Lats1/2 kinase inhibits F-actin binding, cell migration and angiogenesis. *J. Biol. Chem.* **288,** 34041–34051
49. Adler, J. J., Johnson, D. E., Heller, B. L., Bringman, L. R., Ranahan, W. P., Conwell, M. D., Sun, Y., Hudmon, A., and Wells, C. D. (2013) Serum deprivation inhibits the transcriptional co-activators YAP and cell growth via phosphorylation of the 130-kDa isoform of angiomotin by the LATS1/2 protein kinase. *Proc. Natl. Acad. Sci. U.S.A.* **110,** 17368–17373
50. Melkonian, G., Munoz, N., Chung, J., Tong, C., Marr, R., and Talbot, P. (2002) Capillary plexus development in the day five to day six chick chorioallantoic membrane is inhibited by cytochalasin D and Suramin. *J. Exp. Zool.* **292,** 241–254
51. Debefve, E., Pegaz, B., van den Bergh, H., Wagnières, G., Lange, N., and Ballini, J.-P. (2008) Video monitoring of neovessel occlusion induced by photodynamic therapy with verteporfin (Visudyne), in the CAM model. *Angiogenesis* **11,** 235–243
52. Johnson, R., and Halder, G. (2014) The two faces of hippo: targeting the hippo pathway for regenerative medicine and cancer treatment. *Nat. Rev. Drug Discov.* **13,** 63–79
53. Brooke, B. S., Karnik, S. K., and Li, D. Y. (2003) Extracellular matrix in vascular morphogenesis and disease: structure *versus* signal. *Trend Cell Biol.* **13,** 51–56
54. Bonnans, C., Chou, J., and Werb, Z. (2014) Remodeling the extracellular matrix in development and disease. *Nat. Rev. Mol. Cell Biol.* **15,** 786–801
55. Pickup, M. W., Mouw, J. K., and Weaver, V. M. (2014) The extracellular matrix modulates the hallmarks of cancer. *EMBO Rep.* **15,** 1243–1253
56. Yip, K.-P., and Marsh, D. J. (1997) An Arg-Gly-ASP peptide stimulates constriction in rat afferent arteriole. *Am. J. Physiol.* **273,** F768–F776
57. Mogford, J. E., Davis, G. E., Platts, S. H., and Meininger, G. A. (1996) Vascular smooth muscle αvβ3 integrin mediates arteriolar vasodilation in response to RGD peptides. *Circ. Res.* **79,** 821–826
58. Du, X. P., Plow, E. F., Frelinger, A. L., 3rd., O'Toole, T. E., Loftus, J. C., and Ginsberg, M. H. (1991) Ligands activate integrin aIIbβ3 (platelet GPIIb-IIIa). *Cell* **65,** 409–416
59. Legler, D. F., Wiedle, G., Ross, F. P., and Imhof, B. A. (2001) Superactivation of integrin αvβ3 by low antagonists concentrations. *J. Cell Sci.* **114,** 1545–1553
60. Deryugina, E. I., Zajac, E., Juncker-Jensen, A., Kupriyanova, T. A., Welter, L., and Quigley, J. P. (2014) Tissue-infiltrating neutrophils constitute the major *in vivo* source of angiogenesis-inducing MMP-9 in the tumor microenvironment. *Neoplasia* **16,** 771–788
61. Schnoor, M., Cullen, P., Lorkowski, J., Stolle, K., Robenek, H., Troyer, D., Rauterberg, J., and Lorkowski, S. (2008) Production of type VI collagen by human macrophages: a new dimension in macrophage functional heterogenicity. *J. Immunol.* **180,** 5707–5719
62. Jetten, N., Verbruggen, S., Gijbels, M. J., Post, M. J., De Winther, M. P., Donners, M. M. (2014) Anti-inflammatory M2, but not pro-inflammatory M1 macrophage promote angiogenesis *in vivo*. *Angiogenesis* **17,** 109–118
63. Shen, B., Delaney, M. K., and Du, X. (2012) Inside-out, outside-in, and inside-outside-in: G protein signaling in integrin-mediated cell adhesion, spreading, and retraction. *Curr. Opin. Cell Biol.* **24,** 600–606
64. Gong, H., Shen, B., Flevaris, P., Chow, C., Lam, S. C., Voyno-Yasenetskaya, T. A., Kozasa, T., and Du, X. (2010) G-protein subunit Gα13 binds to integrin aIIbβ3 and mediates integrin outside-in signaling. *Science* **327,** 340–343
65. Liao, Z., Kato, H., Pandey, M., Cantor, J. M., Ablooglu, A. J., Ginsberg, M. H., and Shattil, S. J. (2015) Interaction of kindlin-2 with integrin β3 promotes outside-in signaling responses by the αvβ3 vitronectin receptor. *Blood* **125,** 1995–2004
66. von Wichert, G., Jiang, G., Kostic, A., De Vos, K., Sap, J., and Sheetz, M. P. (2003) RPTP-α acts as a transducer of mechanical force on αvβ3-integrin-cytoskeleton linkage. *J. Cell Biol.* **161,** 143–153
67. Somanath, P. R., Malinin, N. L., and Byzova, T. V. (2009) Cooperation between integrin αvβ3 and VEGFR2 in angiogenesis. *Angiogenesis* **12,** 177–185
68. Yu, C.-H., Law, J. B., Suryana, M., Low, H. Y., and Sheetz, M. P. (2011) Early integrin binding to Arg-Gly-Asp peptide activates actin polymerization and contractile movement that stimulates outward translocation. *Proc. Natl. Acad. Sci. U.S.A.* **108,** 20585–20590
69. Tang, Y., Rowe, R. G., Botvinick, E. L., Kurup, A., Putnam, A. J., Seiki, M., Weaver, V. M., Keller, E. T., Goldstein, S., Dai, J., Begun, D., Saunders, T., and Weiss, S. J. (2013) MT1-MMP-dependent control of skeletal stem cell commitment via a β1-integrin/YAP/TAZ signaling axis. *Dev. Cell* **25,** 402–416
70. Kaneko, K., Ito, M., Naoe, Y., Lacy-Hulbert, A., and Ikeda, K. (2014) Integrin αv in the mechanical response of osteoblast lineage cells. *Biochem. Biophys. Res. Commun.* **447,** 352–357